ANALYSIS OF HIGH BURNUP FUEL DURING NORMAL OPERATION, ANTICIPATED OPERATIONAL OCCURENCES, AND DESIGN BASIS ACCIDENTS

A Thesis Presented for the
Master of Science
Degree
The University of Tennessee, Knoxville

Isabelle Ottillia Lindsay
August 2023

ABSTRACT

The US Nuclear Regulatory Commission limits fuel enrichment to 5wt%, effectively limiting the discharge average burnup levels to 62 GWd/MTU. There has been interest in extending the burnup limit beyond 62 GWd/MTU and extending fuel cycles from 18 months to 24 months to improve the economics of large-scale PWRs. It has been shown that in order to increase the cycle length and burnup levels, enrichments above 5wt% are required. Increasing enrichment and burnup levels both present operational performance and safety questions. This work seeks to assess the fuel performance of two fuel designs, both with increased enrichment and implemented burnable absorbers. This work leverages a loose coupling of PARCS, RELAP5-3D, and BISON to evaluate fuel performance during steady state operation, select anticipated operational occurrences, and select design basis accidents. It will address if the current Westinghouse fuel design or the proposed MIT annular fuel design are sufficient to meet criteria described in the NRC SRP during steady state operation, control rod withdrawal scenarios, and control rod ejection scenarios.

TABLE OF CONTENTS

CHAPTER ONE - BACKGROUND AND INTRODUCTION *1*
Supporting background information *1*
Questions and hypothesis *3*
CHAPTER TWO - LITERATURE REVIEW *6*
PNNL report on fuel performance beyond 62 GWd/MTU *6*
Burnable absorbers *11*
NRC licensing process *14*
High burnup experiments and BISON validation *22*
CHAPTER THREE - METHODOLOGY *26*
PARCS *26*
RELAP5-3D *26*
BISON *27*
CHAPTER FOUR - RESULTS *32*
IFBA Core *32*
MIT proposed annular, blended gadolinium fuel design *60*
CHAPTER FIVE - CONCLUSIONS AND DISCUSSION *83*
LIST OF REFERENCES *86*
VITA *93*

LIST OF FIGURES

Figure 1. RELAP5-3D PWR model nodalization. *28*
Figure 2. LHR history for all pins of interest during normal operation for the IFBA core. *35*
Figure 3. Pin A11-1-1 and Pin B10-16-5 maximum fuel and cladding temperatures during steady-state operation. *36*
Figure 4. Pin A11-1-1 and pin B10-16-5 plenum pressure throughout steady-state operation. *.37*
Figure 5. Pin A11-1-1 and pin B10-16-5 cladding hoop strain throughout steady-state operation. *38*
Figure 6. (a) Uncontrolled RCCA bank withdrawal from subcritical or low-power startup condition, and (b) uncontrolled RCCA bank withdrawal at power reproduced from [50]. *40*
Figure 7. (a) HZP CRW and (b) HFP CRW for all pins of interest. *41*
Figure 8. Maximum fuel and cladding temperatures during HZP CRW transients for pin H08-11-4 (highest power) and pin A11-1-1 (highest burnup). *43*
Figure 9: Maximum fuel and cladding temperatures during HFP CRW transients for pin C09-14-13 (highest power) and pin A11-1-1 (highest burnup). *44*
Figure 10. Cladding hoop strain for pin H08-11-4 (highest power) and pin A11-1-1 (highest burnup) during HZP CRW transient and cladding hoop strain for pin C09-14-13 (highest power) and pin A11-1-1 (highest burnup) during HFP CRW transient. *45*
Figure 11. LHR for each pin of interest in a HFP CRE. *47*
Figure 12. LHR for pin A11-1-1 during HFP CRE. *48*
Figure 13. A11-1-1 maximum cladding and fuel temperatures during HFP CRE. *49*
Figure 14. A11-1-1 plenum pressure and cladding hoop strain during HFP CRE. *51*
Figure 15. LHR for pins of interest during HZP CRE. *52*
Figure 16. Selected assemblies of interest for HZP CRE analysis. *53*
Figure 17. LHR experienced for each pin of interest in HZP CRE. *55*
Figure 18. Maximum fuel temperature of each pin of interest during HZP CRE. *56*
Figure 19. Cladding hoop strain of each pin of interest during HZP CRE. *57*
Figure 20. Maximum cladding temperature for each pin of interest during HZP CRE. 5 8
Figure 21. Cladding failure as a function of peak radial average fuel enthalpy rise and excess cladding hydrogen reproduced from [51]. *61*

Figure 22. LHR history for each pin of interest for gadolinium steady state analysis. *63*
Figure 23. Maximum fuel temperature for all pins throughout steady state.....*66*
Figure 24. Maximum cladding temperature for all pins of interest throughout steady state. *67*
Figure 25. Rod internal pressure for each pin of interest during steady state operation.....*68*
Figure 26. Cladding hoop strain for each pin of interest during steady state. *69*
Figure 27. Linear heat rate for HZP CRW for pins of interest. *70*
Figure 28. Maximum fuel temperature for pins of interest during HZP CRW.....*72*
Figure 29. Maximum cladding temperature during HZP CRW for pins of interest. *73*
Figure 30. Maximum cladding hoop strain during HZP CRW for pins of interest. *74*
Figure 31. Plenum pressure during HZP CRW for pins of interest. *75*
Figure 32. Power history for HZP CRE pins of interest. *77*
Figure 33. Maximum fuel temperature observed during HZP CRE for pins of interest. *78*
Figure 34. Maximum cladding temperatures observed during HZP CRE for pins of interest. ...*79*
Figure 35. Maximum cladding hoop strains observed for pins of interest during HZP CRE.....*81*
Figure 36. Plenum pressure observed for pins of interest during HZP CRE. *82*

CHAPTER ONE - BACKGROUND AND INTRODUCTION

Supporting background information

There has been recent interest in increasing average fuel discharge burnups and extend the typical 18-month core operating cycle to a 24-month operating cycle in order to improvement fuel utilization and fuel cycle economics. There are several barriers to this cycle length extension, both from an engineering and a regulatory perspective. Current regulations limit uranium enrichment levels to less than 5 wt%, which effectively limits peak rod-averaged burnup to 62 GWd/MTU [1]. It has been shown that increasing to a 24-month cycle is not possible without an increase in regulatory limits to meet all design goals and constraints as listed by the U.S. Nuclear Regulatory Commission (US NRC) fuel Standard Review Plan (SRP) [2] [3].

Several decades of high burnup fuel testing has revealed high burnup-specific safety concerns, such as corrosive degradation of Zircaloy cladding due to oxidation and hydride accumulation during normal operation [4] [5], high burnup fuel fragmentation (HBFF) during loss-of-coolant accidents (LOCA) [6] [7], and cladding failure induced by pellet cladding mechanical interaction (PCMI) during reactivity-initiated accidents (RIA) [8], all of which are a function of burnup level, cladding temperature, and rod internal pressure [9].

Gap closure is observed due to pellet thermal expansion and cladding creepdown [10]. During operational power ramps or sudden RIAs, the mechanical interaction between fuel pellet and cladding begins to dominate the stress state in the cladding [11][12] [13], which could result in the failure of cladding. Failure of high burnup fuel rods during the initial stages of RIAs and low fuel enthalpies has been observed during RIA-simulating tests on irradiated light water reactor (LWR)-type fuel rods [14] [15] [16] [17] [18] [19]. It was concluded the low-temperature failure mechanism was driven by PCMI combined with cladding embrittlement [20].

Previous efforts to understand PCMI-induced failure mechanism have revealed the correlation between the PCMI-induced failure limit and the oxide layer thickness on the surface of the cladding[21] [22]. They introduced a factor to account for the effect of thickness of the oxide layer on the level of embrittlement of cladding, such as stress intensity factor [22]. However, there is a limited understanding of how transient fission gas release or enthalpy rise impacts PCMI behavior. It has been suggested that fission gas release plays a notable role in the cladding failure during an RIA [23], and studies have that the high burnup structure of the pellet could emphasize fission gas release [24]. It has also been suggested that the energy deposition is proportional to the fuel dimensional change experienced, which determines the stress/strain behavior [13]. In order to better understand contributing mechanisms to PCMI-induced failure, there is a need for a coupled computational analysis that utilizes neutronics, thermal-hydraulics, and thermo-mechanics.

Computational analysis for high burnup fuel during RIA transient has been highlighted in RIA code benchmarks [25] [26] using different codes that are validated against experimental databases from the NSRR and CABRI programs, which will be discussed later. It was concluded that uncertainty in the cladding and coolant heat transfer and cladding loading boundary conditions, such as the gap closure and liftoff during PCMI, were the primary drivers for differences between the codes. Studies have also highlighted that for better prediction of fuel behavior during an RIA, there is a need to investigate uncertainties regarding high burnup fuel characteristics such as “fission gases distribution, fuel microstructure, clad corrosion state, and gap conductance” [27]. Thermomechanical responses during RIA were found to be conservative when not taking high burnup features into consideration [28] [29]. However, the prediction of high burnup fuel behaviors has been improved by updating heat transfer parameters between

fuel, gap, and cladding [30], applying dynamic gap model [31], or refining transient FGR model and boiling curve parameters [32]. Another approach to address the limitations is to couple the fuel performance analysis with neutronics and/or thermal hydraulics analysis for more precise and realistic safety analysis. Previous work using BISON provided better predictions of fuel behavior when a more accurate input of the power histories during RIA was fed from VERA, the core simulator [33].

Capps et al. [34] demonstrated the feasibility of coupling between BISON, RELAP5-3D, and VERA, applicable to the analysis of high burnup fuel behavior during LOCA conditions. This work will build on this study by simulating Control Rod Withdrawal (CRW) scenarios and RIA scenarios using high burnup fuels at various stages of life. This work will utilize a currently existing fuel design by Westinghouse and a proposed fuel design by MIT. This work will utilize PARCS, a neutronics code; RELAP5-3D, a thermal-hydraulics code; and BISON, a fuel performance code.

Questions and hypothesis

Understanding there is a need for 24-month to improve the economics of PWR's, the safety implications need to be addressed before moving forward in the licensing process. In order to meet licensing standards of fuel, fuel temperature, cladding temperature, cladding strain, rod internal pressure, cladding oxidation, cladding hydride accumulation, and fuel enthalpy need to be addressed. As discussed, it is understood that higher enrichment is necessary to meet the demands of 24-month cycles. Moving forward, utilities can utilize fuel designs that are already used in the industry, or they can adopt new fuel designs that were created with the 24-month cycle in mind. This work addresses several questions relating specifically to fuel performance in 24-month cycles.

The first question addressed is, “Is the current Westinghouse IFBA fuel design with increased enrichment up to 6.6 wt% and burnup up to 73 GWd/MTU sufficient to meet design requirements?” Current NRC guidance specifically addresses fuel performance for fuel enrichments of 5 wt% ^{235}U, which is the limiting factor in extending fuel cycle length. In this work, the fuel enrichment levels in this design are increased up to 6.6 wt%, but it is assumed the same fuel performance limitations apply. It is likely that some guidelines are not limiting enough at higher burnups and will need to be adjusted in the future, but this issue is outside of the scope of this work. Instead, general performance analyses will be performed, and conclusions will be drawn in a conservative manner. Understanding that the release of helium as the boron layer is depleted will result in drastic increases in plenum pressures, it is likely certain limitations, such as the 1% cladding strain limit, will be exceeded, making the fuel design insufficient to implement in 24-month fuel cycles

This leads to the second question, which is, “Is the MIT annular, gadolinium doped fuel design acceptable in a 24-month cycle?” As discussed, using gadolinium as a burnable absorber has several benefits. Gadolinium does not produce additional gas when absorbing a neutron, and combined with another volume for gas to populate, the likelihood of excessive plenum pressures and cladding strains is reduced. A consequence of doping fuel with a burnable absorber is decreased thermal conductivity throughout the fuel. This will lead to higher fuel and cladding temperatures, however it is unlikely the temperature limits given by the NRC are met or exceeded, as they are generous.

An additional goal of this work is the gain an understanding of key factors when evaluating high burnup fuel performance and performance of fuel with enrichments higher than 5wt%. Knowing that high burnup pins will be shuffled to the outer periphery of the core, it is

likely that burnup will not be the limiting factor when considering fuel performance. Instead, it is possible that the higher enrichment at the early stages of life results in greater enthalpy depositions, which will result in higher fuel and cladding temperatures, which will be challenging to the fuel.

These questions and this goal will be addressed using a loose coupling of neutronic (PARCS), thermal hydraulic (RELAP5-3D), and fuel performance (BISON) codes. Each code will simulate steady state operation, an AOO event, and a DBA event. The addressed AOO event is a control rod withdrawal (CRW) from both hot zero power and hot full power. The selected DBA event is a control rod ejection (CRE) from both hot zero power and hot full power.

CHAPTER TWO - LITERATURE REVIEW

PNNL report on fuel performance beyond 62 GWd/MTU

In 2019, Pacific Northwest National Laboratory published a report on fuel performance needs for extending rod average discharge burnup limits above 62 GWd/MTU for the NRC [2], as the NRC is anticipating licensing applications for burnup extensions in LWR systems. This report provides a summary of high burnup phenomena in fuel, gap region, and cladding as well as potential changes to safety analysis codes and methods. The report discusses currently available data and potential data gaps and performance concerns.

High burnup phenomena

High burnup fuel exhibits a few differences in performance beyond 62 GWd/MTU. The report discusses changes to fission gas release in fuel that has not failed, changes to failed fuel fission gas release, high burnup rim development, changes to thermal conductivity, changes to the fuel melting point, thermal conductivity changes, fuel swelling during operation, fuel swelling in spent fuel storage, and changes to the power distribution across the pellet radius [2].

Regarding the changes to fission gas release in intact fuel and failed fuel, generally, the rate of release increases with higher burnups [2]. Generally, fission gas is released at a fraction of 1% per 10 GWd/MTU at low power and 3-4% per 10 GWd/MTU at high power [2]. However, beyond 60 GWd/MTU, the release fraction increases exponentially, with 15% observed by 80 GWd/MTU and 22% is observed by 100 GWd/MTU. Fission gas release impacts plenum pressure directly, which influences cladding behavior. Increased fission gas release is the primary impact of higher burnup on the gap region, as it can contribute to the gap reopening at high burnup. If the gap reopens, fuel temperature could increase, contributing to further fission gas release and lower gap conductance.

The high burnup rim is characterized by “submicron grains with low angle grain boundaries and high porosity” [2] and is developed by 40 GWd/MTU burnup. As burnup increases, the thickness of the rim increases exponentially. The high porosity of the high burnup rim allows this region of the fuel to hold a large amount of fission gas. In the occasion of a design basis event, this fission gas could be released and impact cladding deformation behavior. Additionally, during LOCA induced ballooning and burst, the submicron grain size could lead to increased pellet fragmentation. The pellet fragmentation could lead to coolability challenges during both LOCA and RIA events.

As a ceramic material, UO_2 has notably poor thermal conductivity, as the heat transfer is facilitated by phonon heat transfer or lattice vibrations [2]. As void and interstitials develop, they interfere with the material lattice and radiation damage creates dislocations in the lattice, limiting heat transfer by lattice vibrations. Because the heat transfer is limited, higher fuel temperatures are exhibited.

A decrease in thermal conductivity limits heat transfer to the coolant and leads to increased fuel temperatures. High fuel temperatures leave less of a differential between the temperature of the fuel and the fuel melting point. The fuel melting point decreases 1-5°C per GWd/MTU, and this decreases the safety margin for fuel performance [2].

Increased fuel swelling is observed in normal operating and long-term dry storage as burnup increases [2]. This is largely due to solid fission products within the fuel. Fuel swelling increases at a linear rate with burnup and is higher at high burnups than at beginning of life. The increase in swelling can contribute to higher rod internal pressures, which can contribute to cladding deformation and failure behavior in severe accidents.

Increased burnup also impacts the power production profile across the radius of the fuel pellet [2]. At the beginning of pellet life, the power is somewhat uniform with a small peak near the surface. However, as burnup increases, the peak at the pellet edge increases due to self-shielding and plutonium production. This pronounced peak contributes to further burnup peaking near the edge of the pellet. High burnup on the edge of the pellet influences thermal conductivity and can interfere with temperature profile predictions. Temperature predictions are important for fission gas release predictions, which influence many fuel performance metrics, such as plenum pressure and therefore cladding strain.

Fuel cladding is impacted by fast neutron fluence and long-term exposure to cooling water [2]. Most notably, the yield stress and tensile strength of zirconium-based claddings increase up to two times the unirradiated value. Beyond 50 GWd/MTU, the strengthening effects saturate. Beyond this strengthening effect, irradiation does not have significant impact on cladding creep.

When the cladding is exposed to water over a long period of time, the zirconium chemically reacts with the water, creating zirconium oxide and free hydrogen [2]. This effectively thins the cladding. The free hydrogen can be absorbed and precipitate into hydrides within the cladding region, embrittling the cladding

Currently available data

The PNNL report discusses currently available data for fuel with burnups higher than 62 GWd/MTU. The report discusses “in-reactor fuel temperature tests, power ramp tests, and RIA tests” [2]. Additionally, the report also discusses out-of-reactor analyses of “fission gas release, cladding corrosion and hydriding, cladding mechanical properties, and LOCA tests” [2].

The in-reactor fuel temperature tests discussed were performed at the Halden reactor. The Halden reactor was a heavy water moderated thermal reactor in Norway. The major purpose of this reactor was to generate operational safety data to be used in the extension of fuel utilization and to understand the degradation of core materials due to water effects and irradiation. Three notable tests [2] from the Halden reactor were IFA-562 Rod 18, IFA-597 Rod 8 and IFA 515.10. These tests were irradiated to 76 GWd/MTU, 71 GWd/MTU, and 80 GWd/MTU respectively. The available data captures temperature behavior well up to 70 GWd/MTU, but there is notably less data available between 70 and 85 GWd/MTU.

Ramp tests provide insight into cladding strain caused by a rapid increase in power. In these tests, fabricated fuel segments were irradiated to a specified burnup level and then the segments were exposed to substantial power increases. Ramp tests that provide data relevant to high burnups were the B&W Studsvik power ramps and the SCIP-1 Ramp tests. These tests were performed at 62 GWd/MTU and 72 GWd/MTU, respectively. At the time of this report, there was substantial power ramp data up to 72 GWd/MTU, but no data beyond 72 GWd/MTU [2].

RIA tests were completed at the CABRI reactor and the Nuclear Safety Research Reactor (NSRR). The CABRI reactor is a pressurized water loop capable of replicating power pulse conditions to help understand fuel behavior during fast transients. The NSRR is a TRIGA-type reactor that is also capable of replicating power pulses. The experiments performed at CABRI and NSRR supplement data sufficiently up to 80 GWd/MTU and provide enough data to assess failure limits associated with high burnup levels.

Fission gas release data is collected out-of-reactor, post irradiation. Generally, low power rods exhibit low fission gas release while high power rods exhibit higher fission gas release. in fission gas release data collection, it is desirable to evaluate high power rods with release

fractions, as this will drive rod internal pressure. There is a significant amount of data available for burnups of up to 70 GWd/MTU, but there is a limited amount of data between 70GWd/MTU and 100 GWd/MTU [2].

Regarding cladding corrosion and hydriding, there is very limited data available in the public domain. The PNNL report recommends that experimental data and model calculations to rationalize and defend high burnup are included in applications. However, regarding cladding mechanical properties, there is sufficient data available up to 72 GWd/MTU. There is limited data relevant to mechanical behavior between 72 GWd/MTU and 85 GWd/MTU. If an applicant uses a proprietary design, this report recommends they should provide proprietary high burnup data that supports the licensing of high burnup fuel [2].

Integral LOCA tests have demonstrated there is some pellet fragmentation and relocation from rods that have burst above 60 GWd/MTU, but a significantly greater amount at burnup levels of 80 GWd/MTU. This could challenge radiological release and coolability limits for both LOCA scenarios and RIA scenarios [2].

Data gaps and performance concerns

The PNNL report concludes that there are many areas that will necessitate more data and that there are a number of performance concerns. The primary performance concerns are oxidation and hydriding of the cladding, stress and strain limits, fission gas release and rod internal pressure, LOCA post quench ductility, RIA cladding failure, fuel fragmentation, and spent fuel storage and transportation. To help confirm that current regulatory limits are sufficient or to better inform new regulatory limits for high burnup fuels, data should be generated up to 85 GWd/MTU in the areas described below [2]:

- Fuel centerline temperature data between 70 GWd/MTU and 85 GWd/MTU
- Power ramp data above 72 GWd/MTU
- Fission gas release data beyond 70 GWd/MTU
- Cladding corrosion and hydriding behavior data beyond 70 GWd/MTU
- Cladding mechanical behavior beyond 72 GWd/MTU

The work described in this thesis utilizes BISON, which is validated the available experimental studies for high burnup, including the Halden reactor experiments, the CABRI tests, and the NSRR tests. The work will show a current understanding of PWR fuel behavior at high burnups using the available data.

Burnable absorbers

As mentioned, it is not possible to extend the length of the fuel cycle to 24 months without also increasing the fuel enrichment. However, this leads to additional excess reactivity during the early stages of life of the fuel. This creates a need to suppress this reactivity to limit power peaking in the core. Control rods can be used to suppress reactivity, but inserting control rods deep into the core can cause further non-uniformity. Instead, burnable absorbers can be used to absorb excess neutrons and thus suppress excess reactivity and extend fuel cycles [35].

Burnable absorbers are materials that are non-fissile but have a large neutron absorption cross section [36]. As they absorb excess neutrons, the abundance of burnable absorbers decreases. As the abundance decreases, so does the impact of the burnable absorber. Common burnable absorbers include lithium, boron, silver, cadmium, indium, samarium, europium, gadolinium, dysprosium, erbium, lutetium, hafnium, and indium.

Soluble neutron absorbers are routinely used in the primary coolant loop of commercial PWRs, creating a uniform negative reactivity throughout the core. The use of soluble absorbers is restricted because they degrade the void coefficient of reactivity of the moderator. To supplement them and to localize neutron absorption, absorbers are integrated into LWR fuel assemblies.

Examples of non-fueled rodlet designs are the "Westinghouse Wet Annular Burnable Absorber (WABA) and the Borosilicate Glass (BSG) burnable absorber" [37]. The WABA rod is an annular rod that encases the burnable absorber between two zircaloy tubes. The BSG rod is similar, but instead of zircaloy tubes, it uses stainless steel.

There are three ways burnable absorbers can be introduced to fuel rods. The first is to incorporate the burnable absorber homogenously throughout the fuel pellet, the second is to add a layer of burnable absorber on the surface of the fuel pellet, and the third way is to combine the first two. Traditionally, because boron is the most commonly used burnable absorber, the release of helium from the $^{10}B(n,\alpha)^{7}Li$ reaction needs to be considered. This accumulation of boron within the fuel leads to a reduction of the thermal conductivity of the fuel, increased fuel temperature, and an acceleration of fission gas release. Therefore, boron is only used in the second method of incorporation, where a thin layer is applied on the surface of the fuel rod [38].

Westinghouse developed a type of fuel known as Integral Fuel Burnable Absorber (IFBA) fuel. In this design, a thin layer of boron is sprayed onto the fuel pellets during production before the pellets are encased in cladding [37]. This layer can vary in thickness between 1 and 5 μm and the enrichment of ^{10}B can vary as well. As mentioned, a consequence of the $^{10}B(n,\alpha)^{7}Li$ reaction is the release of helium, but in this design it is released into the gap and plenum region instead of the fuel matrix. The release of helium contributes to excessive plenum

pressures, which may affect cladding performance and the ability of the fuel to meet safety criteria later in its life. To account for this increase in plenum pressure throughout the fuel lifetime, the initial plenum pressure is decreased from typical rod fill pressures to 0.7 MPa instead of the typical 1.26 MPa. Additionally, because the boron is only a thin layer on the outer surface of the fuel, it depletes quickly, typically within the first 30 MWd/kgU of burnup.

To avoid the increase of rod internal pressure, the first method of incorporating burnable absorbers into fuels should again be considered, but with an isotope that does not release a gas. The use of gadolinium resolves the issue of gas accumulation as the absorption of a neutron simply produces a heavier form of gadolinium, while still being a strong neutron absorber. Additionally, because it is mixed homogenously throughout the fuel pellet, it depletes throughout the lifetime of the fuel. The addition of gadolinium does, however, lower the thermal conductivity of the fuel, which can result in high centerline temperatures throughout the fuel region and a reduction in heat removal to the coolant, making the overall system slightly less efficient [39]. Historically, gadolinium has been incorporated of levels of up to 8 wt%.

Work is currently being performed to study the effects of adopting a higher enrichment, annular fuel design that incorporates gadolinium as a burnable absorber at Massachusetts Institute of Technology to meet the performance needs of high burnup fuel. The use of annular fuel helps address issues with fission gas release and therefore plenum pressure. The addition of a central fill gas region provides an additional surface for fission gas release. However, the central region of the fuel is the area of highest temperatures, making it the region of highest fission gas diffusion rates. In this design, the center annular region is optimized to minimize fission gas release.

NRC licensing process

In order for a nuclear power plant to operate, a license from the NRC is required. The NRC uses two licensing processes that are applicable in different scenarios [40]. The first licensing process is outlined in Title 10 Of The Code Of Federal Regulations Part 50 (10 CFR 50) and is a two-step process. The first part of 10 CFR 50 is the construction permit. The construction permit contains preliminary safety analyses, an environmental review, financial statements, and an assessment of the need and demand of the plant. If it is determined that the construction permit application contains all necessary information, the NRC publishes a "notice of receipt." At this point, the NRC acknowledges the application to be complete and begins the review process. This includes a thorough review of the site safety characteristics and emergency planning, and which is included in a safety evaluation report [40].

While in review, the NRC hosts public meetings near the proposed site of the power plant. The purpose of these meeting is to support public participation in the licensing process, provide an opportunity for the public to become familiar with the "safety and environmental impacts of the design" [40], and provide a platform for the public to provide feedback. Independent of the NRC, the Advisory Committee on Reactor Safeguards (ACRS) reviews each construction permit application and the safety evaluation associated with the application. This is also hosted in a public meeting and reported back to the NRC. Another public meeting is held by an Atomic Safety and Licensing Board, which is composed of a lawyer and two qualified experts, during which public members may submit statements, either oral or written, to be included in the hearing record.

During this time, the NRC conducts an environmental review. This review discusses positive and negative impacts of building the plant. This review feeds into the draft environmental impact statement, which is issued to the public and government agencies. After

any comments are collected, the NRC issues a Final Environmental Impact Statement (FEIS) to address them [40]. Assuming all requirements are met during this phase, a construction license is granted.

During the construction of the plant, operation plans are developed, and the applicant applies for an operating license from the NRC. This application is the second part of 10 CFR 50. The applicant includes a final safety analysis report (FSAR) and an updated environmental safety report within this application. The FSAR describes the power plant's "final design, operational limits, anticipated response of the plant to postulated accidents, and emergency response plans" [40]. The NRC, along with the Federal Emergency Management Agency, reviews the FSAR and determines whether or not the plans are adequate. The ACRS reviews the operating license application and FSAR in a public meeting. After review, if all requirements are met, an operating license is granted.

10 CFR 52 is considered a combined licensing process. In this process, the operating license is granted as part of the preliminary design certification and/or the Early Site Permit (ESP). The ESP licenses a site without committing to the construction of a plant or a specific design. It is composed of four major requirements: the site safety analysis report, the environmental report, the site redress plan, and a major features emergency plan. The ESP is valid for 20 years, with the opportunity to renew beyond 20 years.

The design certification is a way for the NRC to review and approve a design for a substantial portion of a nuclear power plant and incorporate the design into regulations while the final details are finalized.

Compared to other methods, the design certification is subject to more restrictive change processes. In the design control document, two "tiers" must be complete. The first tier is the part

of the design the NRC certifies and includes the “Inspections, Tests, Analyses, and Acceptance Criteria (ITAAC), site parameters, and interface requirements” [40]. The second tier, which is only changeable with NRC approval, is design-supporting information used in the NRC review. When the design is heavily dependent on changing technology and procurement information, the Design Acceptance Criteria (DAC). This is applicable to things such as piping, digital controls, and human factors.

The use of a combined license provides a single licensing action for both the construction and operating license, thus saving a significant amount of time in the overall process. It needs to demonstrate that the total design falls within ESP or design certification defined parameters and have a description of the site-specific probabilistic risk assessment and technical specifications. Additionally, the ITAAC must be defined, which is the largest tradeoff for the single-licensing action. As discussed earlier, the ITAAC verifies the plant will be constructed and operated in correspondingly with the design the NRC approved.

This work uses two core designs for Southern Nuclear’s Vogtle Electric Generating Plant (VEGP) units 1 and 2. VEGP units 1 and 2 are Westinghouse 4-loop reactors with 1229 MWe gross capacity. Construction began in 1976 and were commissioned in 1987 and 1989, respectively. In order to obtain an operation license, Southern Nuclear submitted an FSAR in accordance with NUREG-0800, SRP. The SRP provides guidance to the NRC for reviewing safety reviews, such as the Preliminary Safety Analysis Report (PSAR) and FSAR, when considering construction permit applications and operating license applications.

The SRP [3] serves two main purposes. The first is to assure consistency of staff safety reviews. Secondly, it makes information available in order to improve communication between

the NRC, public, and industry. These purposes improve understanding of the NRC's review process. There are 19 chapters in the SRP, each discussing a specific scope of review.

Chapter 4 section 2 of the SRP discusses the fuel system design [3]. The analyses in this section evaluate the fuel system thermal, mechanical, and materials design during normal operation, transient scenarios, and accident scenarios. The areas of review confirm a few things. First, it confirms fuel damage does not occur during normal operation or in Anticipated Operational Occurrences (AOOs). Additionally, it assures the fuel damage that could occur in more severe scenarios does not prevent control rods from being inserted, the number of fuel rod failures is properly estimated, and coolability is maintained.

To meet these guidelines, the NRC has developed a set of acceptance criteria. Generally, during normal operation, stress limits for components should be provided, the number of strain fatigue cycles on the structural components should be notably less than the design lifetime, and fretting wear, oxidation and hydriding (crud), dimensional changes to fuel components should be limited. Otherwise, plenum pressure should remain below the system operational pressure during steady state operation and AOOs, evaluation of the effects of worst-case hydraulic conditions during steady state operation and AOOs should be performed on the fuel system, and control rod insertability and reactivity must be maintained [3].

It should be noted that there are exceptions described to some of these criteria. Pertinent to this work, the criteria describing rod internal pressure states that it should remain below the system operation pressure or "another limit that is properly justified" in the safety analysis reports. The following requirements describe a minimum criterion for a different limit [3]:

1. It is shown that cladding liftoff should not occur during normal operation

2. It is shown that cladding hydrides should not reorient in the radial direction
3. A “description of failures due to departure of nucleate boiling (DNB) resulting from excess fuel rod pressure” is provided [3]

SRP also describes acceptance criteria for fuel rod failure. This section states that it must be ensured that fuel does not fail during normal operation or AOOs. Fuel rod failure is permissible in accident scenarios, but this failure must be accounted for in the radiological release analysis. It is noted that it is impossible to prevent all fuel failures during steady state operation. Therefore, it should be demonstrated that systems are in place to accommodate for small leaks [3].

In the acceptance criteria for fuel rod failure, the SRP describes what should be addressed in the safety analysis, listing possible failure modes of fuel. In total, there are eight modes described: “hydriding, cladding collapse, cladding overheating, fuel overheating, excessive fuel enthalpy, pellet-cladding interaction, cladding bursting, and mechanical fracturing” [3].

Hydriding is a result of moisture within the zirconium alloy component and can happen internally or externally. In 1989, internal hydriding was cited as a persistent cause of cladding failures, resulting from small defects [41]. Work shows that the significant factors affecting internal hydriding were the “defect hole size, internal and external sources of hydrogen, zircaloy surface properties, nickel alloy contamination of Zircaloy, heat flux and fluence” [41]. In order to prevent internal hydriding and address these factors, the SRP requires that fuel and cladding are manufactured to have no more than 20μg/g (20 ppm) moisture. External hydriding is a result of the waterside corrosion of the zirconium alloy and is not prevented. It is only limited by the initial moisture content and the limitation of defects.

Cladding collapse is a result of fuel densification, which leaves a gap between the cladding and fuel. If the cladding collapses into the gap, it is assumed to fail due to high local strains. Failure of the fuel due to overheating of the cladding is assumed to not occur if thermal margin criteria, described in the thermal and hydraulic design portion of the SRP, are met.

Excessive fuel enthalpy refers to the energy suddenly increasing during a RIA, which could lead to PCMI. Due to the rapid energy deposition during an RIA, the fuel rapidly increases in temperature, resulting in thermal expansion. This can result in PCMI, which refers to the mechanical interaction of the expanded fuel pellet and the inner surface of the cladding. This can deform the cladding to the point of rupture [42]. High burnup fuel PCMI during RIAs is documented from experiments conducted at NSRR [43]. This work showed a reduction in the failure threshold for enthalpy increases. In fuel that was below 42 MWd/kgU burnup, fuel integrity was demonstrated up to 453 J/g enthalpy, but in fuel of 50 MWd/kgU burnup, fuel failed below the failure threshold described in Japanese safety guidelines (456 J/g). When analyzing fuel of high burnup, it is important to note that because of the reduction in failure threshold, more conservative estimates should be made.

There are two different types of pellet/cladding interaction. PCMI is primarily a stress driven phenomena that is a result of volumetric expansion of the fuel against the inner surface of the cladding. Pellet-Cladding Interaction (PCI) can be caused by cracking of the cladding as a result of fission product embrittlement. These two phenomena are similar and are addressed in the same manner in the documentation [3]. There is currently no criterion for pellet/cladding interaction induced failure, but there are general guidelines described in the SRP. The first is that cladding strain should not exceed 1%. The second guideline is that fuel melting should be

avoided. This is due to the large volume increase that is associated with fuel melt, which could exert additional stress on the cladding.

Bursting refers to the swelling and rupture of fuel cladding due to excessive heat in the cladding and the pressure differential between the fuel rod and coolant pressure. NUREG-0630 describes an acceptable rupture-temperature vs. differential-pressure curve.

Mechanical fracture is caused by a force on the external surface of the cladding, such as hydraulic load or core-plate motion. If stress applied to the cladding is no greater than 90% of the irradiated yield stress, it is assumed integrity is maintained. If the applicant chooses to use a different limit, it should be justified.

The last area of design bases described in the SRP fuel system design section is a description of fuel coolability. Fuel coolability is only applicable in postulated accident scenarios and should be covered in chapter 15 of the PSAR/FSAR. Traditionally, fuel is considered of coolable geometry if the assembly retains rod-bundle geometry, i.e., the cladding does not fail to the point of disrupting the bundle, with sufficient coolant channels in order to remove residual heat from a postulated accident. A reduction in coolability can be caused by a number of instances including expulsion of fuel, cladding embrittlement, structural deformation, cladding melting, and fuel rod ballooning.

The four aspects that should be addressed for complete criteria are expulsion of fuel, cladding embrittlement, fuel rod ballooning, generalized cladding melting, and structural deformation [3]. The cladding embrittlement limitations are that the maximum cladding temperature experienced must remain below 2200°F, or 1477.6 K, and that the oxidation remains below 17%. Violent expulsion of fuel can occur in severe RIAs and is a result of mechanical interaction. The mechanical action should be address and there are several mechanisms that can

lead to mechanical failure that are described in the fuel failure section. Generalized cladding melt can cause a loss in rod-bundle geometry. Understanding that the cladding melting temperature is higher than 1477.6 K, it does not need to be addressed specifically, as the cladding embrittlement criteria are more conservative. When addressing fuel rod ballooning, Regulatory Guide 1.157 describes applicable methods that can realistically calculate ballooning behavior during a LOCA. Because this thesis work focuses on reactivity-initiated events, fuel rod ballooning is not heavily discussed. In non-LOCA accidents, fuel rod ballooning can be a result of rod internal pressure exceeding system pressure, which is discussed in the fuel failure section. Structural deformation can be addressed by a number of analytical procedures that are listed in appendix A of the SRP.

The SRP also includes an interim acceptance criteria and guidance for RIAs in Appendix B [3]. This section simplifies the earlier sections, specifically for reactivity-initiated events Regarding fuel cladding failure, Appendix B recommends fuel rods with an internal rod pressure equal to or lower than the system pressure have a peak radial average fuel enthalpy limit of 170 cal/g at hot zero power. For rods with plenum pressures exceeding the system pressure, the limit is 150 cal/g. At power levels between 5% and 100% rated thermal power conditions, cladding is assumed to fail if "local heat flux exceeds thermal design limits" [2]. The core coolability criteria are reduced to a maximum radial average fuel enthalpy limit of 230 cal/g, a maximum fuel temperature limit of melting conditions, an addressing of mechanical energy generated, and a requirement of no loss of coolable geometry. In this interim guidance, the NRC staff developed a correlation between the increase in fuel enthalpy and fission gas release,

$$Transient\ FGR = [(0.2286 * \Delta H) - 7.1419$$

Where:

$$FGR = \ Fission\ gas\ release, \%, \geq 0$$

$$\Delta H = Increase\ in\ fuel\ enthalpy, \frac{\Delta cal}{g}.$$

High burnup experiments and BISON validation

BISON was developed using fundamental behaviors and relationships developed from experimental data. For each experiment BISON is validated against, there is a data set and input deck associated with the test. BISON is frequently modified and updated, so this set of BISON inputs is run on a daily basis to assure the results calculated by BISON and the experimental results are in acceptable agreement.

There is an extensive list of experiments BISON is validated against. All information in this section of this review is from the BISON documentation in [45]. The most relevant validation cases for this work are the high burnup cases, which include:

- IFA-562.2 tests
- IFA-597.3 tests
- RIA CABRI REP Na 2 3 4 5 and 10 tests

IFA-562

The IFA-562.2 tests were part of the Ultra High Burnup program, and the goal was to provide temperature data throughout the fuel pin's life. The rods used in these tests were annular rods enriched to 13wt% U-235 and were irradiated for 2.68 years to obtain an average burnup level of 50 GWd/MTU. For each analyzed pin, the experimental temperature results and the

results predicted by BISON agree very well. For rod 15 and rod 16, the predicted results were within 3% and 2% of the measured result, on average, respectively. One note is that BISON generally overpredicted the fuel centerline temperature at higher temperatures and burnups. In rod 17, the results are in even better agreement with the predicted results being within 1.5% of the measured results. In all three cases, there were root mean squared error values close to 1 [45].

IFA-597.3

The IFA-597.3 test validations use results from two rods. The rod 8 test was first conducted at the Halden reactor and used a Ringhals boiling water reactor rod that was refabricated for the experiment [45]. Rod 7 was based on rod 8, and the two rods and tests were very similar. The main difference between rod 7 and rod 8 is that rod 7 was instrumented with an elongation detector. The tests on the rods were conducted at similar powers, but the 2 kW/m difference is somewhat significant as the maximum power was only 30 kW/m. The goal of these experiments was to understand fuel temperature, cladding elongation, and fission gas release at higher burnups.

For the fuel temperature predictions, there is reasonable agreement between the measured values and the BISON predicted values. The available comparison for this validation does not provide a specific average relative error or root mean squared error, but it does demonstrate that all values are within 10% relative error, which is acceptable per the study [45]. Regarding fission gas release, BISON is shown to underpredict the total amount at the end of irradiation and power ramps. BISON predicts cladding elongation for both glued and frictionless simulations and the experimental results lie between the results of those simulations.

RIA CABRI REP Na 2, 3, 4, 5, and 10 tests

The CABRI RIA tests were a set of tests to provide understanding of fuel behavior during RIAs. All four tests were performed using 17x17 UO_2 type fuel with Zy-4 cladding. The test vary in fuel enrichment and maximum burnup. REP Na 3, 4, 5, and 10 each have initial enrichments of 4.5% and maximum burnup levels of 53.8 GWd/MTU,64 GWd/MTU, 64, GWd/MTU, and 63 GWd/MTU, respectively. However, the REP Na-2 test was performed using an enrichment level of 6.85% and a maximum burnup level of only 33 GWd/MTU. This higher enrichment and lower burnup results in a greater energy deposition compared to the other three tests. The REP Na 2 test experienced an energy deposition of 207 cal/g, while the lower enrichment, higher burnup cases experienced energy depositions between 95 cal/g and 122.2 cal/g.

The experimental results of the CABRI tests are limited without membership to the CABRI International Program, so the simulations of these tests are validated against FALCON results obtained from EPRI reports and the available experimental results. For REP Na-2, there is reasonable temperature results agreement with all results being within 10% of available FALCON and experimental results. However, the mechanical behavior comparisons vary much more significantly. When compared to the FALCON and experimental results, BISON underpredicts hoop strain and cladding displacement, but over predicts fission gas release. The BISON team attributes the difference in mechanical behavior to the implementation of the frictionless contact model and acknowledges further development of the non-frictionless model is valuable. Transient and high burnup fission gas release models have since been developed in BISON and better predict fission gas release behavior Similar behavior is observed in REP Na-3,

-4, -5, and -10 where temperature behavior is reasonably predicted but mechanical behavior has significant variation.

BISON validation takeaways

The primary takeaways from the BISON validation work are that for normal operation, BISON does an adequate level of predicting temperature and mechanical behavior; however, during an RIA simulation, while BISON predicts temperature behavior well, it does not predict mechanical behavior as effectively. With this understanding, it is necessary to draw more conservative conclusions when interpreting mechanical behavior results from the simulations in this thesis.

CHAPTER THREE – METHODOLOGY

Capps et al. [34] demonstrated the feasibility of coupling between BISON, Reactor Excursion and Leak Analysis Program—Three Dimensional (RELAP5-3D), and VERA as the analyses tools for high burnup fuel behavior during LOCA conditions. Building on this study, this work seeks to employ a loose coupling of PARCS, RELAP5-3D, and BISON to answer the questions posed. This work is a piece of a larger project, which seeks to address the safety-implications of 24-month cycles using high burnup fuel. The project is a multi-institutional effort with several individuals focusing on various pieces.

PARCS

PARCS is a deterministic 3D spatial kinetics core simulator code used to predict system and local response to normal operation and transient conditions. PARCS is especially suited for analyzing RIAs for which core flux distribution and key safety-related peaking factors may vary significantly. Additionally, it provides the ability to reconstruct pin power information to perform pin-wise evaluations of limiting factors for safety analysis purposes. Because of these advantages, the NRC uses PARCS for neutronics analyses of proposed reactor designs. These advantages also make PARCS an effective tool for safety analyses in the evaluation of RIAs and can be used in this work. The Polaris lattice physics code [35] was used in this study to conduct deterministic transport and fuel depletion calculations for generating the few-group cross sections needed for PARCS.

RELAP5-3D

The thermal hydraulic responses of HBU fuel rods were analyzed using RELAP5-3D for the transient conditions. The RELAP5-3D code was developed at Idaho National Laboratory (INL) [44] and is a deterministic system code with the multidimensional capability to model

operational transients and postulated accidents in reactor systems. RELAP5-3D employs a partially implicit numerical scheme to solve partial differential equations for mass, momentum, and energy for two-phase systems. Several generic component models are included in the code, such as pumps, valves, pipes, heat structures, separators, pressurizers, and control system components. RELAP5-3D can also account for the special phenomena—such as form loss and boiling heat transfer—using user-input variables. Figure 1 illustrates the nodalization scheme of a four-loop Westinghouse PWR that consists of four fuel pins and a core-average region built in RELAP5-3D. Each pin represents specific HBU fuel pins at various locations in the core obtained from PARCS simulations. Previous work performed in Capps et al. [34] demonstrated the capability of steady-state analysis for the four-loop Westinghouse PWR using a one-pin model, with one heat structure representing the pin of interest and the other heat structure representing the rest of the core. This paper extends it to a four-pin model to analyze the thermal-hydraulic responses of four different HBU fuel pins during transient conditions.

BISON

BISON is a nuclear fuel performance code developed and maintained by INL and uses a finite-element solve method [45]. BISON solves systems of partial differential equations to evaluate fuel t thermal properties, fission gas production, thermal and irradiation creep, swelling, and fracture. Models are implemented to evaluate plasticity, irradiation growth, thermal and irradiation creep, gap heat transfer, thermal and mechanical contact, plenum pressure and volume, and gap gas temperature.

During steady state operation, the zircaloy cladding oxidizes by undergoing a chemical reaction with the water coolant [46], as shown in equation 1.

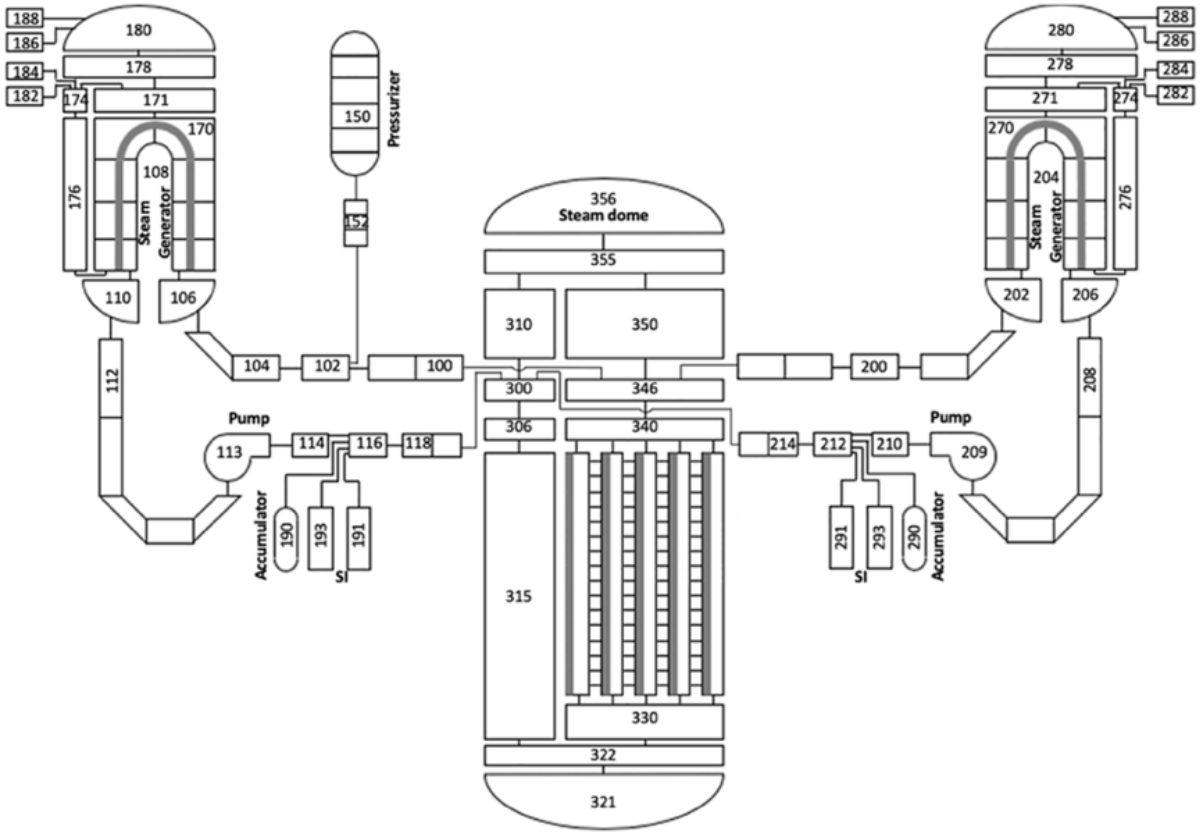


Figure 1. RELAP5-3D PWR model nodalization adapted from [34].

$$Zr + 2H_2O \rightarrow ZrO_2 + 2H_2 \quad (1)$$

The oxidation model employed calculates the oxide layer development at both operating and high temperatures. At normal operating temperatures, oxidation is calculated by considering the pretransition oxidation process and the post-transition oxidation process. The pretransition period oxidation rate follows a cubic time dependence given by

$$\frac{dS^3}{dt} = C_1 \exp\left(-\frac{Q_1}{RT_I}\right), for\ S \leq S_{trans}, \quad (2)$$

and the post-oxidation rate follows a linear time dependence given by

$$\frac{dS}{dt} = C_2 \exp\left(-\frac{Q_2}{RT_I}\right), for\ S > S_{trans}, \quad (3)$$

where "S is the oxide thickness, T_I is the metal-oxide interface temperature, C_1 is the rate constant for pretransition oxidation, Q_1 is the activation energy for pretransition oxidation, C_2 is the rate constant for post-transition oxidation, Q_2 is the activation energy for post-transition oxidation, R is the universal gas constant, and S_{trans} is the transition oxide thickness" [45]. The transition thickness is the thickness where the oxidation rate stops following a cubic time dependence and begins following a linear time dependence, which is typically approximately 2 μm [47]. The metal-oxide interface temperature is the temperature between the developed oxide layer and the unaffected Zircaloy and is found using the coolant temperature (T_{co}), the thermal conductivity of zirconium oxide (K_{ox}), the oxide thickness (S), and the heat flux (q"). The relationship is given by equation 3.

$$T_I = T_{co} + \frac{q''S}{k_{ox}}. \quad (3)$$

A byproduct of the oxidation is excess hydrogen, which can diffuse into the cladding. Because hydrogen solubility in zircaloy is low, the zircaloy matrix can become supersaturated with hydrogen. If this occurs, the hydrogen can embrittle the cladding. In the event of a transient, the embrittled cladding can fail, leading to the release of fission products into the coolant system [48]. A model was developed and implemented into the fuel performance code, BISON, which can help assess the hydrogen content of fuel cladding throughout operation. The model utilizes hydrogen flux, hydride precipitation and dissolution, and precipitation kinetics models to predict the hydrogen content and hydrogen as hydride contents of cladding [49].

The hydrogen flux can be described by Fick's diffusion and the Soret effect. Fick's diffusion describes the flux as a function of the concentration gradient, and the Soret effect describes the flux as a function of the temperature gradient. The total hydrogen flux is the sum of these two primary effects, which are dependent on diffusion coefficients that are dependent on the material, hydrogen concentration, temperature, and the heat of transport. These relationships are described by:

$$J_{tot} = J_{Fick} + J_{Soret} = -D\nabla C_{ss} - \frac{DC_{ss}Q^*}{RT^2}\nabla T \quad (4)$$

D is the mentioned diffusion coefficient, which is dependent on the activation energy of hydrogen diffusion in Zircaloy and temperature and can be described by equation 5, where A_D and E_D are constants defined in the Bison model as 7.9e-7 m^2/s and 4.49e4 J/mole respectively [49].

$$D = A_D \exp\left(-\frac{E_D}{RT}\right) \tag{5}$$

The precipitation and dissolution relationships are proportional to the concentration of hydrogen and are dependent on temperature. They are different due to the presence of the hysteresis region.

$$TSSP\ [wt.ppm] = 138746.0 \exp\left(-\frac{4145.72}{T}\right) \tag{6}$$

$$TSSD\ [wt.ppm] = 106446.7 \exp\left(-\frac{4328.67}{T}\right) \tag{7}$$

When considering transient behavior, the precipitation rate is considered. The precipitation rate, S, is implemented using the Marino model, where α is a kinetics parameter that describes the temperature dependence [49].

$$S = \alpha^2(C_{SS} - TSSP) \tag{8}$$

$$\alpha == 62.3\left[s^{-\frac{1}{2}}\right] exp\left(-\frac{4.12*10^4\left[\frac{J}{mol}\right]}{RT}\right) \tag{9}$$

The Bison model also considers the change in the hydrogen concentration as described by equation 10. θ describes the volume fraction of hydrogen in the α phase and Φ describes the volume fraction of hydrides compared to total hydrogen [49].

$$\frac{\delta\theta C_{ss}}{\delta t} = -\nabla \cdot \theta J_{tot} - \theta S \tag{10}$$

$$\frac{\delta\Phi}{\delta t} = \frac{\mathrm{M_{ZrH1.66}}}{\mathrm{M_H}} \frac{\theta \mathrm{S}}{1.66} \tag{11}$$

The volume fraction can be artificially reduced by the user by using the clamping factor, Φ. The clamping factor limits the maximum volume fraction of hydrides permitted [49].

$$\theta = 1 - \frac{\Phi}{f_{clamp}} \tag{12}$$

CHAPTER FOUR - RESULTS

IFBA Core

IFBA Steady State

The pins selected capture the highest burnup in the center of the core, highest burnup on the edge of the core, average power, peak power, maximum temperature during the transient, and maximum temperature increase throughout the transient based on the PARCS calculations. The pins considered for analysis are summarized in Table 1. The pins are labelled in column 1 as the assembly location in the core and the [*x*,*y*] location within the assembly. The HBU pins could be limiting due to cladding embrittlement and therefore have a higher likelihood of cladding failure. Peak power, maximum temperature during the transient, and maximum temperature increase throughout the transient could be limiting due to the higher likelihood of fuel melting. In total, nine scenarios were considered.

PARCS provided the fuel linear heat rate (LHR) history, shown in Figure 2, and fuel axial peaking factors for all pins of interest. Histories for coolant pressure and coolant temperature were developed using operational constants. Coolant pressure was defined as 15.5 MPa at full power and 0.1 MPa (atmospheric pressure) during fuel shuffling periods. Coolant temperature was defined as 565 K at full power and 293 K (room temperature) during fuel shuffling periods. The fuel performance parameters of interest when evaluating coolability are fuel and cladding temperature, plenum pressure, and hoop strain. The main driver for fuel thermal response is pin power, which was determined by the LHR and the axial peaking factor. For this reason, the pin with the highest power was analyzed to capture the results of the most strenuous conditions during steady-state operation. The highest pin power corresponds to pin B10-16-5. Pin A11-1-1 was determined to have the highest end-of-steady-state burnup over the core and was analyzed to capture the relationship between burnup and fuel performance.

Table 1. Pins considered for detailed thermomechanical analysis.

Assembly [Pin *x*, Pin *y*]	Parameter	Case	Number of cycles
H09 [5,4]	HBU (center)	All	2
A11 [1,1]	HBU (edge)	All	3
H08 [11,4]	Peak power, max temperature, max temperature rise	HZP EOC	1
B10 [16,5]	Average power	HFP EOC	1
H08 [10,9]	Max temperature	HFP EOC	1
G09 [13,14]	Max power	HFP EOC	1
C09 [14,13]	Max temperature rise	HFP EOC	1

Figure 3 shows the increases and decreases in fuel temperature that correspond to increases and decreases in LHR. Both pins experienced similar behavior during their respective first fuel cycles. The maximum fuel temperature in B10-16-5 is higher than the maximum fuel temperature in A11-1-1 due to a higher LHR, with maximum fuel temperatures of 1389 K and 1326 K respectively. Throughout the life of the fuel, heat transfer properties through the gap region and in the outer region of the fuel degrade because of HBU structure development, which is relevant during the second and third fuel cycles for pin A11-1-1. This degradation causes fuel temperatures to remain relatively constant during the second fuel cycle when the LHR decreases. The centerline temperature decreases by approximately 200 K in the third cycle. The maximum cladding temperature is maintained between 610 K 640 K for both pins during steady state operation.

Plenum pressure (Figure 4) increases with burnup due to solid fission product accumulation and fuel thermal expansion, which leads to pellet-cladding gap closure and decreases the total plenum and gap volume and further increases plenum pressure. During the first approximately 20 GWd/MTU of burnup, the layer of boron in the gap region is burned, releasing helium and lithium into the gap region. This causes a rapid initial increase in plenum pressure, which then slows after the boron has been depleted. Hoop strain (Figure 5) initially decreases because of cladding creepdown in the first fuel cycle. Pin B10-16-5 begins to experience and increase in hoop strain during its first fuel cycle due to the higher temperatures observed in the fuel, leading to quicker thermal expansion compared to A11-1-1. During the first fuel shuffle sequence, compressive hoop strain is observed, which results in a decrease in temperature. During the second and third fuel cycles during which the gap region is closed, expansive hoop strain is observed and increases as the fuel radially expands.

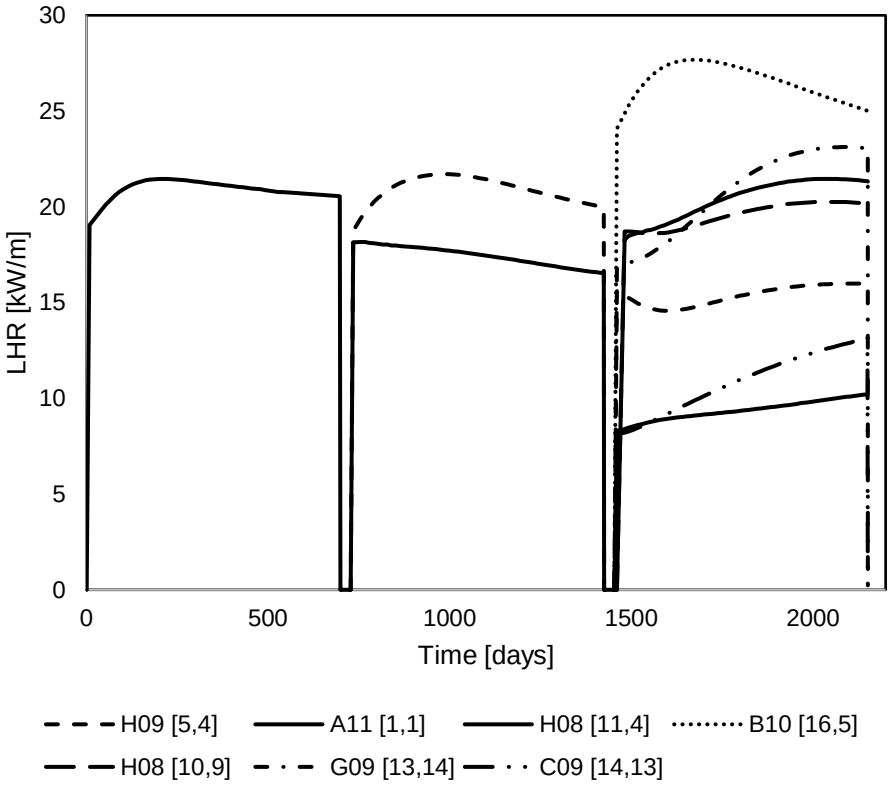


Figure 2. LHR history for all pins of interest.

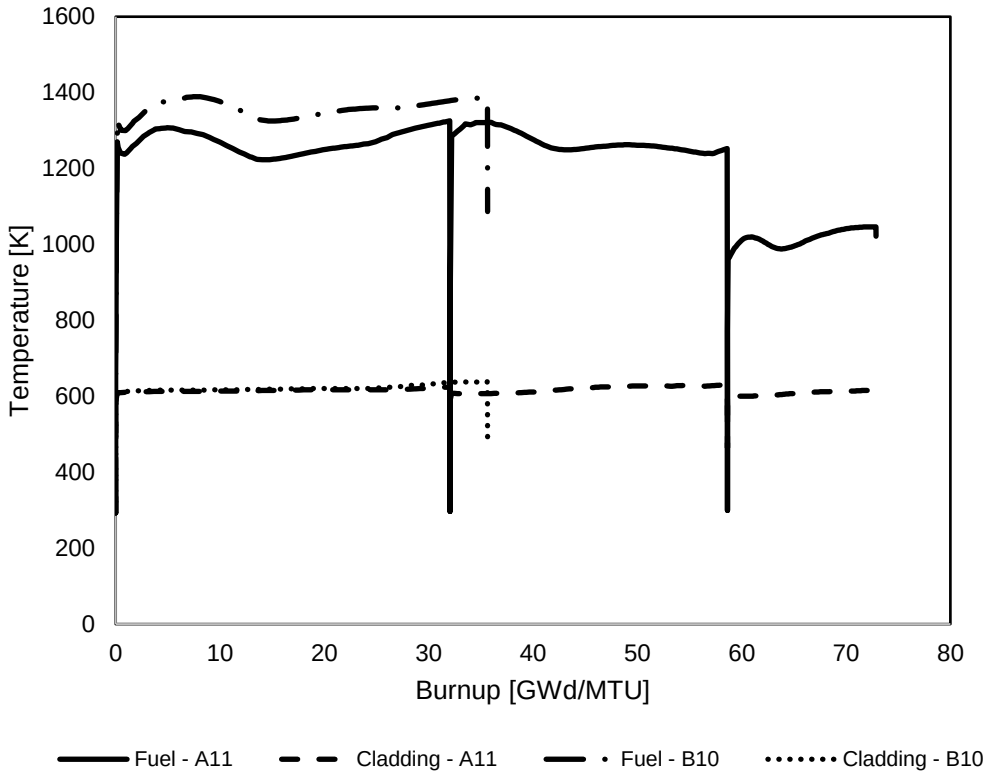


Figure 3. Pin A11-1-1 and Pin B10-16-5 maximum fuel and cladding temperatures during steady-state operation.

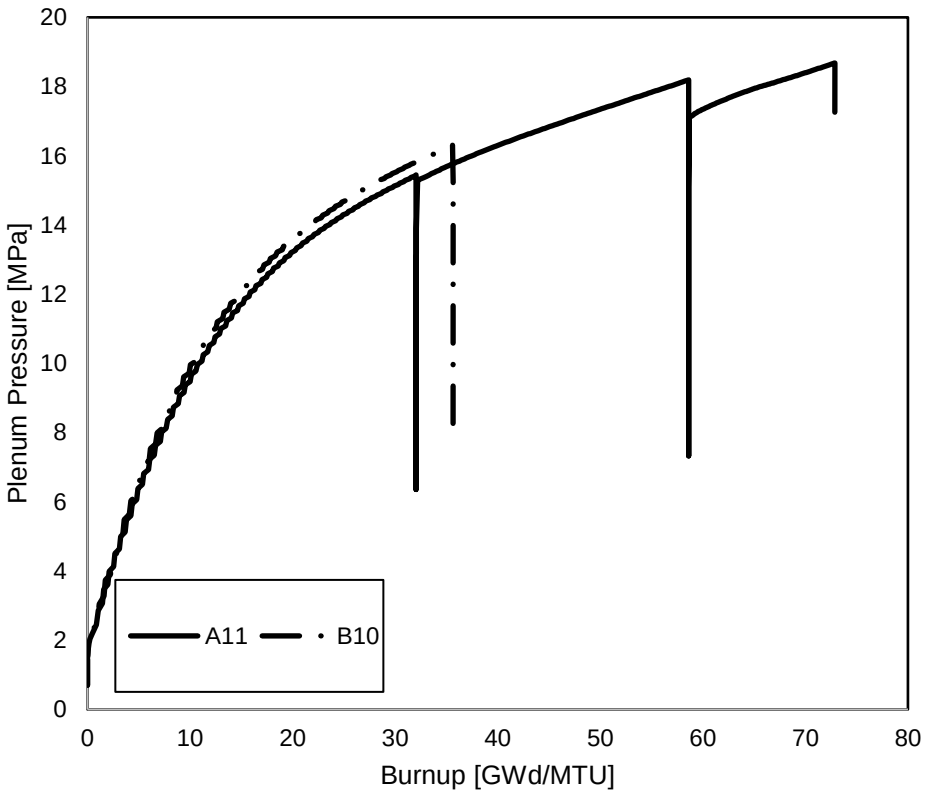


Figure 4. Pin A11-1-1 and pin B10-16-5 plenum pressure throughout steady-state operation.

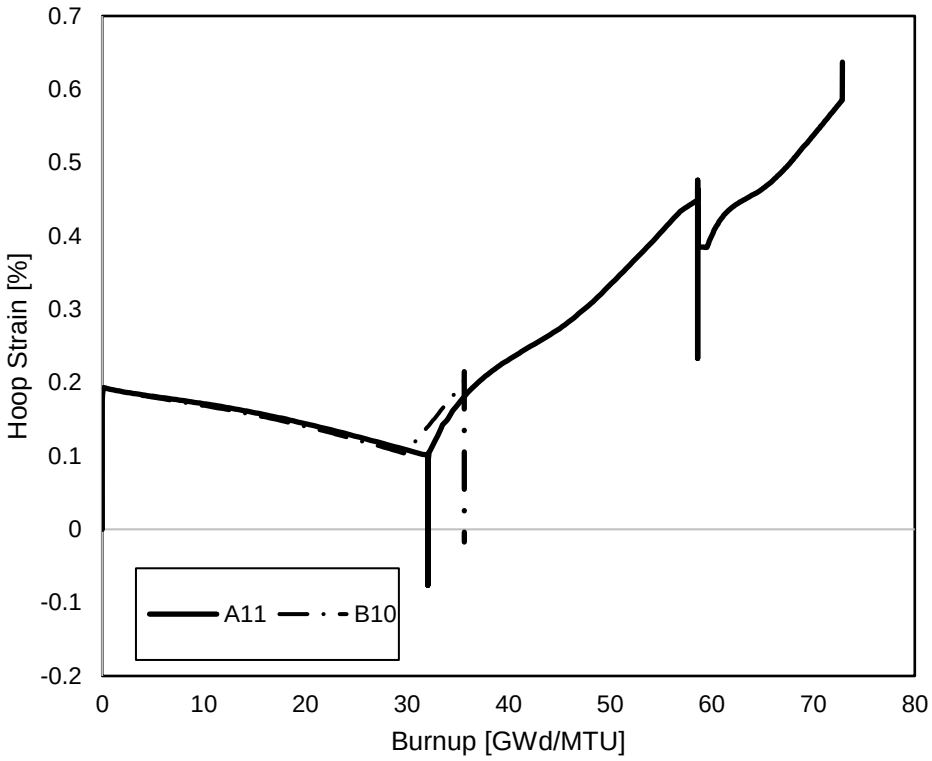


Figure 5. Pin A11-1-1 and pin B10-16-5 cladding hoop strain throughout steady-state operation.

IFBA CRW

Chapter 15 of the Vogtle Electric Generating Plant *Final Safety Analysis Report* (FSAR) [50] outlines the analyses of a plant's response to postulated safety-related events, including a CRW. Two transients discussed are an "uncontrolled rod cluster control assembly (RCCA) bank withdrawal from subcritical or low-power startup condition" (Figure 6a) and an "uncontrolled RCCA bank withdrawal at power" (Figure 6b) [50]. Throughout the remainder of this work, the former scenario is described as a *hot zero power (HZP) CRW*, and the latter is described as a *hot full-power (HFP) CRW*. CRWs are AOOs, and because they are assumed to occur during the lifetime of the plant, stricter safety criteria must be met. In AOOs, fuel must be able to return to normal operation. For fuel to return to normal operation, it must be structurally intact with limited damage.

During the CRW transients, the relevant fuel parameters are fuel and cladding temperature, fuel and cladding deformation, and radial enthalpy. PARCS provided the transient fuel LHR behavior, shown in Figure 7, and fuel axial peaking factors for each pin of interest during both scenarios to RELAP5-3D. RELAP5-3D provided the coolant boundary conditions, temperature, and pressure to BISON, along with the power profile from PARCS. For transient analysis, the pins with the highest LHR and highest burnup during the transient were considered. For HZP conditions, this corresponds to pin H08-11-4 for the highest LHR and pin A11-1-1 for the highest burnup. In HFP conditions, this would correspond to pin C09-14-13 and pin A11-1-1, respectively.

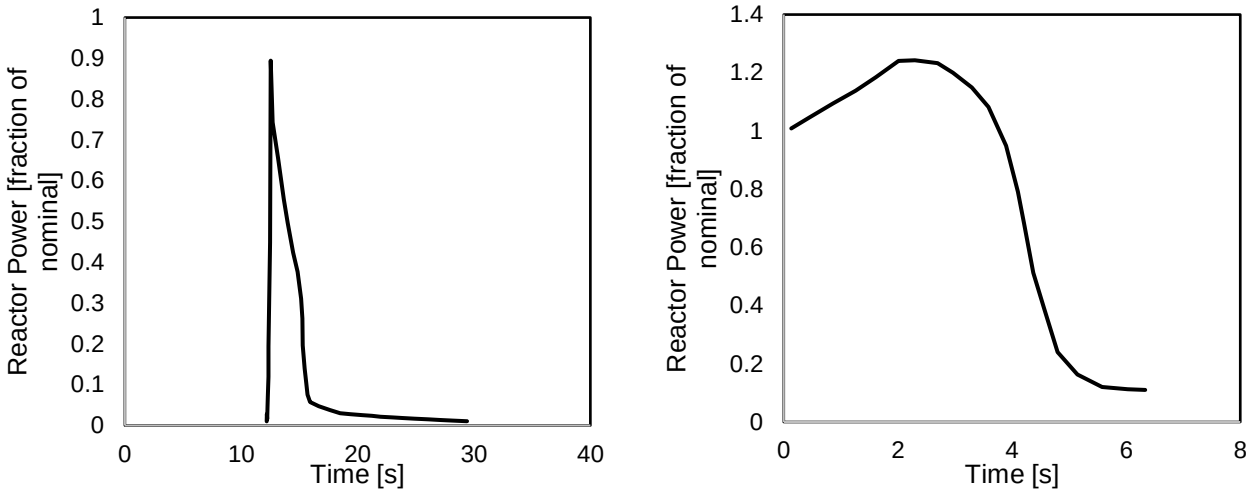
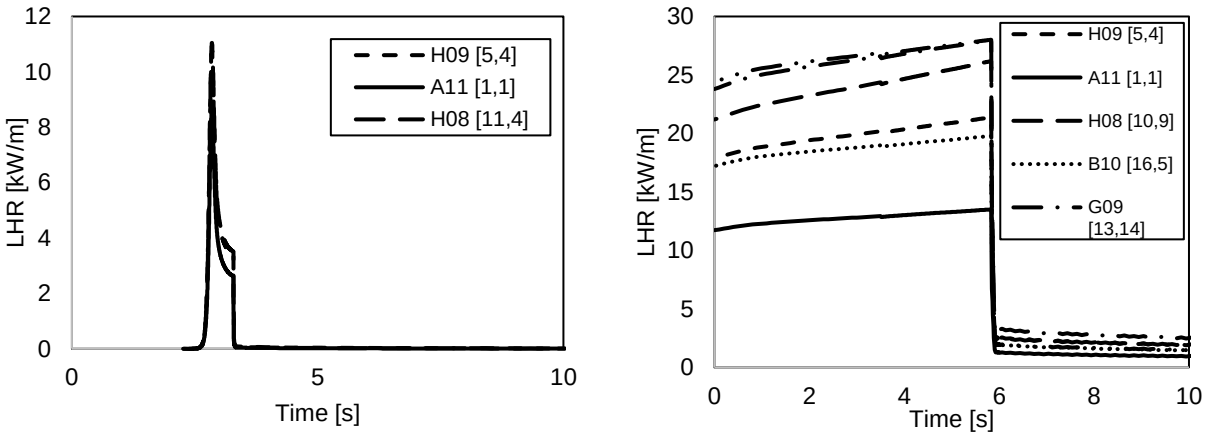


Figure 6. (a) Uncontrolled RCCA bank withdrawal from subcritical or low-power startup condition, and (b) uncontrolled RCCA bank withdrawal at power from [50], integrated into VEGP core design.



(a) (b)

Figure 7. (a) HZP CRW and (b) HFP CRW for all pins of interest.

Figure 8 and figure 9 show the maximum fuel and cladding temperature throughout the transients. Similar to the steady state, there is a is a corresponding increase and decrease in fuel and cladding temperature to the increase and decrease in LHR. Of the two transients, HFP was more drastic and produced a maximum fuel temperature of 1,372 K in the high-power scenario and 1,127 K in the HBU scenario. The cladding temperature reached maximums of 656 K and 636 K, respectively. The fuel temperature is below the fuel melting point, and the cladding temperature is below the coolability limit by significant margins.

Fuel and cladding deformation can be evaluated via cladding hoop strain. High cladding hoop strain indicates thermal expansion in the fuel region. Figure 10 summarizes the maximum cladding hoop strain behavior throughout both transient conditions. In HZP conditions, negligible hoop strain behavior is observed in both pins. The HBU pin maintains cladding hoop strain at 0.5% throughout the transient, which is less than observed hoop strain during the steady-state analysis. The high-power pin, however, maintained a compressive hoop strain. This is due to the compressive behavior of the cladding during shutdown and is similar to the behavior of the analyzed steady-state pins during fuel shuffle sequences. In HFP conditions, the HBU pin experiences the highest cladding hoop strain with a slight increase 0.08%, reaching a maximum of 0.62%. The high-power pin experiences an increase of 0.15%, reaching a maximum of 0.21%. These strain increases are both less than observed during reactor startup in the steady-state portion of this work, indicating that this fuel rod is not expected to fail or experience enough deformation to prevent subsequent steady-state full-power operation. The maximum enthalpy observed between all scenarios was 256.7 J/g, which is equivalent to 61.4 cal/g.

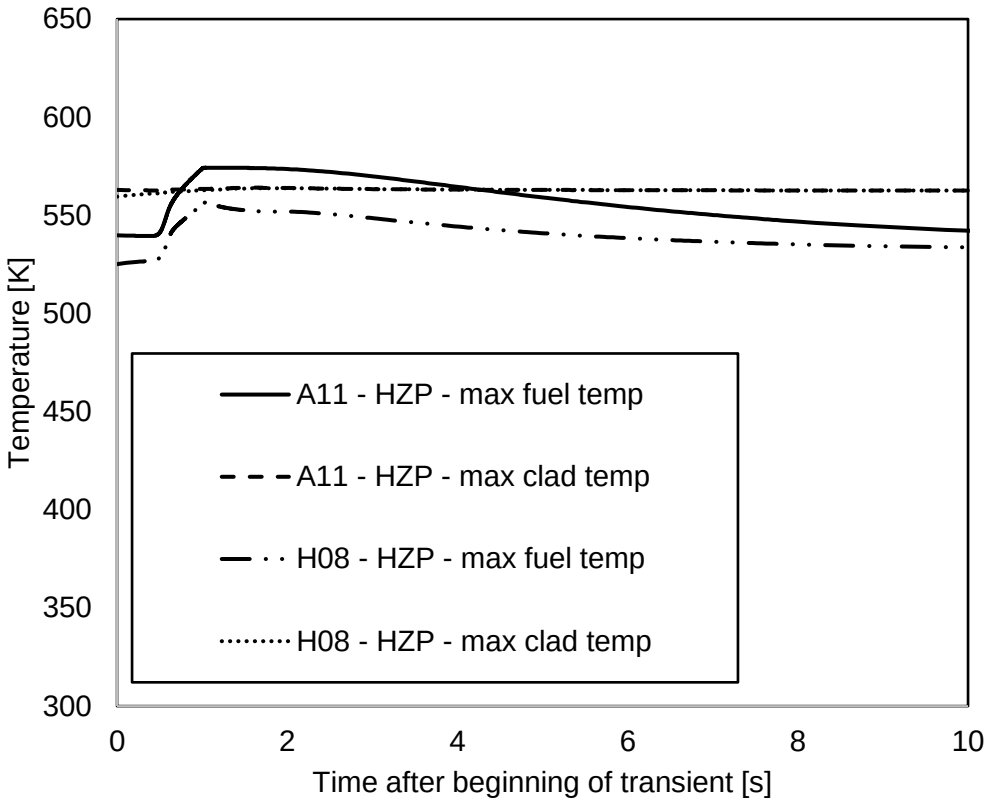


Figure 8. Maximum fuel and cladding temperatures during HZP CRW transients for pin H08-11-4 (highest power) and pin A11-1-1 (highest burnup).

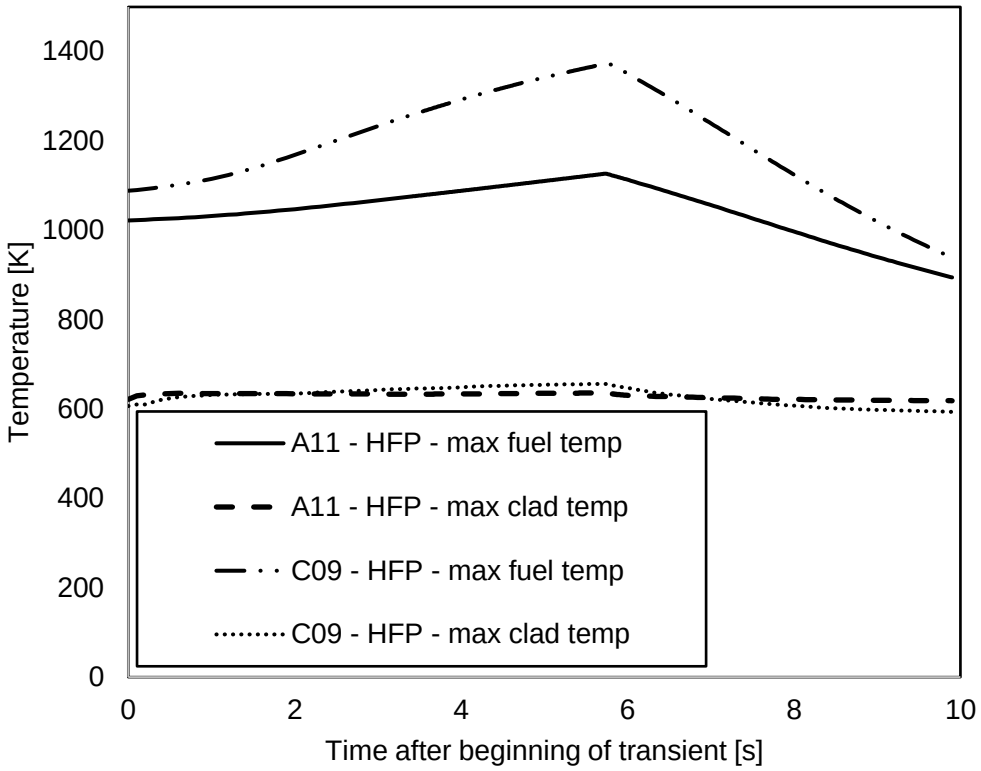


Figure 9. Maximum fuel and cladding temperatures during HFP CRW transients for pin C09-14-13 (highest power) and pin A11-1-1 (highest burnup).

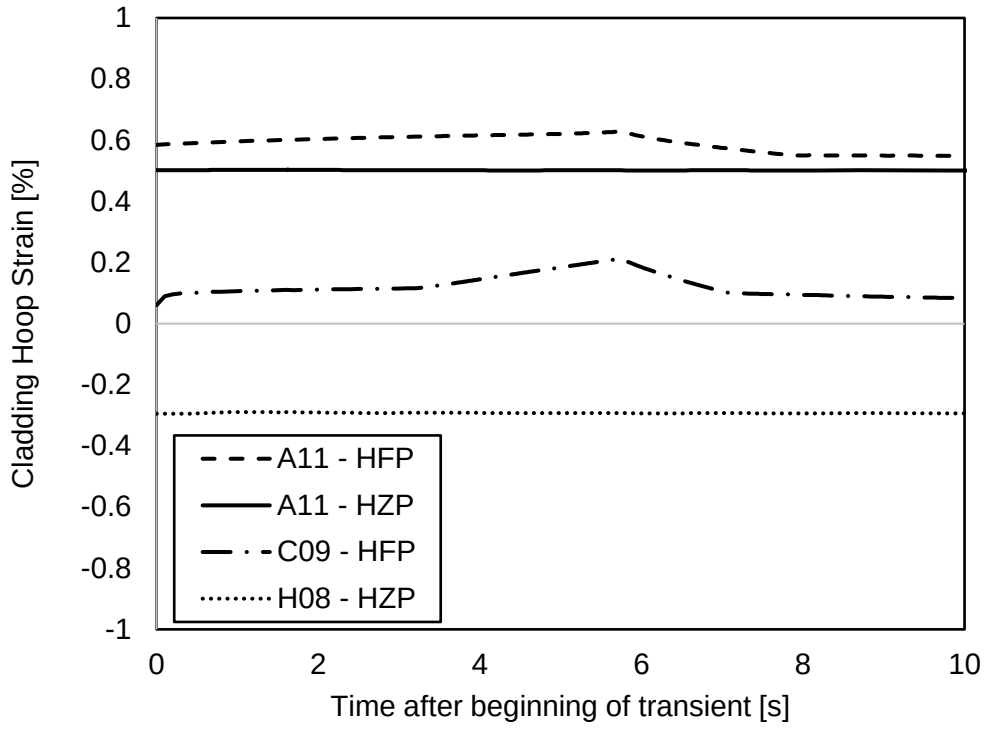


Figure 10. Cladding hoop strain for pin H08-11-4 (highest power) and pin A11-1-1 (highest burnup) during HZP CRW transient and cladding hoop strain for pin C09-14-13 (highest power) and pin A11-1-1 (highest burnup) during HFP CRW transient

IFBA CRE

A CRE is defined as the ejection of a rod of the control rod and drive shaft due to the control rod mechanism pressure housing failure[50]. The consequence is a rapid reactivity insertion with an unfavorable core power distribution. This could possibly lead to localized fuel rod damage. This work assumes the rod with the greatest worth is ejected and addresses both HFP and HZP conditions.

IFBA HFP CRE

The power conditions for the most limiting pins in the HFP CRE scenario are shown in figure 11, and each will be analyzed in the future. For now, the fuel pin with the highest burnup is considered, which is end of cycle A11-1-1. This pin is a thrice-burned pin, with its assembly starting towards the center of the core in the first two cycles and moving to the periphery for the last fuel cycle.

For the transient portion of the analysis, PARCS provided the LHR (figure 12) and APF boundary conditions, similar to the CRW analysis. Because the analyzed pin was in the periphery region of the core, this specific pin does not experience an aggressive LHR increase during a CRE, as the ejected rod is closer to the center of the core. While coolant temperature and pressure were determined using operational constants in the steady- state portion of this analysis, RELAP5-3D was used to develop the TH boundary conditions for the transient analysis. Figure 13 shows the maximum fuel and cladding temperatures throughout the transient. Similar to the steady-state case, there is a corresponding increase and decrease in maximum temperatures to the increase and decrease in LHR. The maximum fuel and cladding temperatures throughout the transient were 1,138 K and 642 K, respectively.

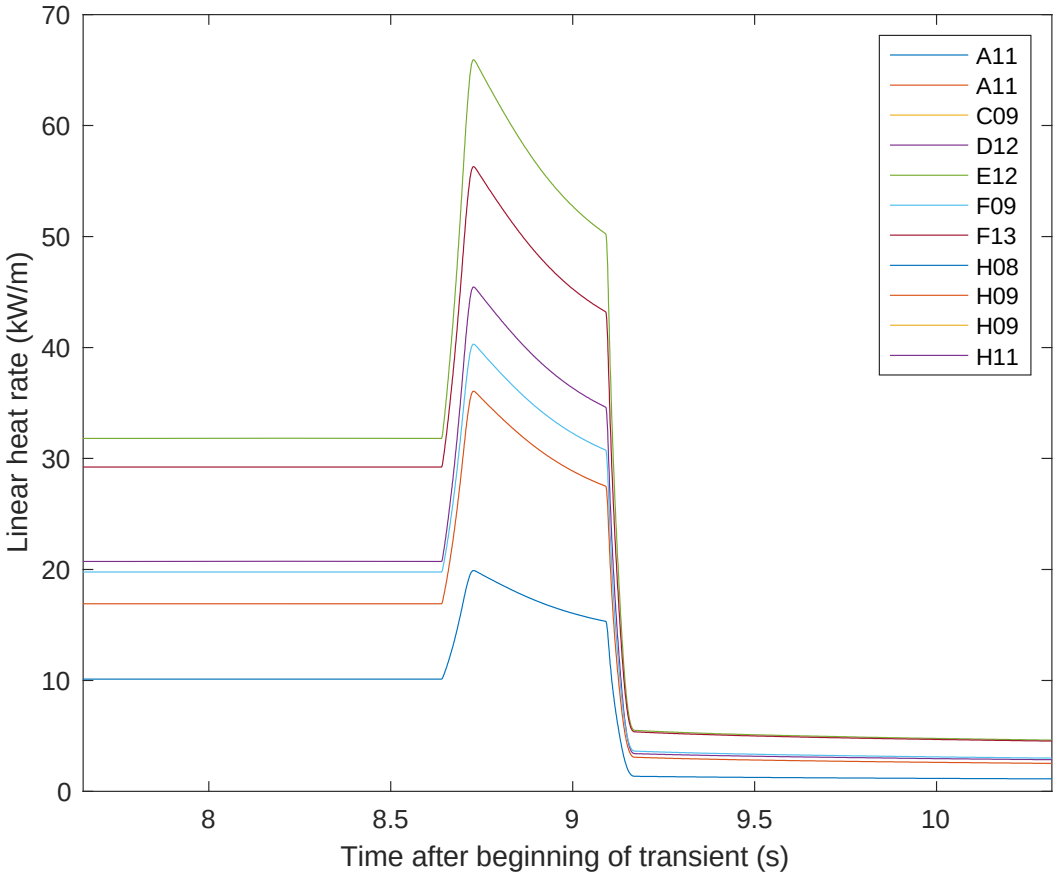


Figure 11. LHR for each pin of interest in a HFP CRE.

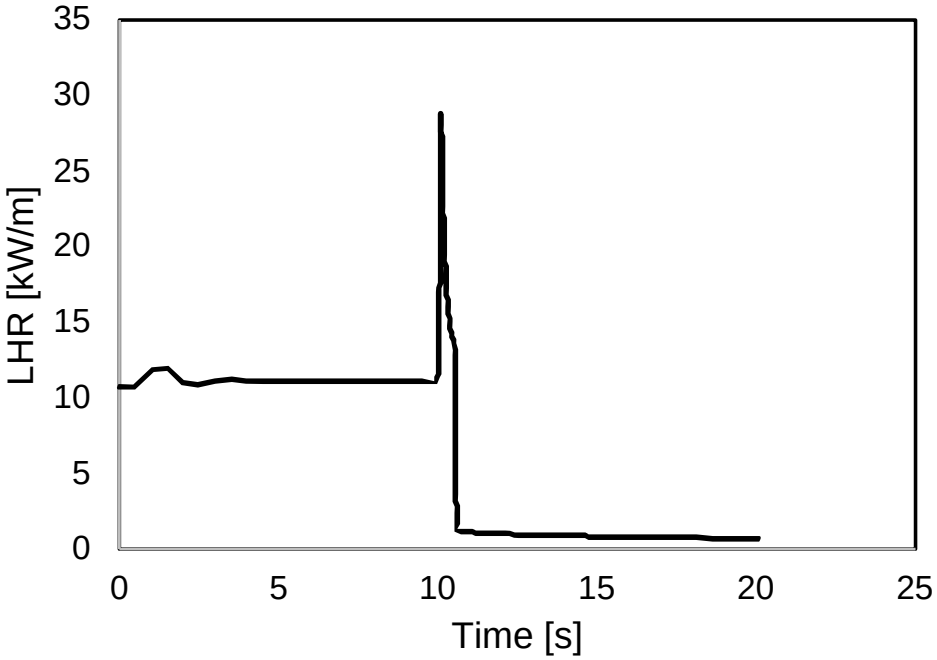


Figure 12. LHR for pin A11-1-1 during HFP CRE.

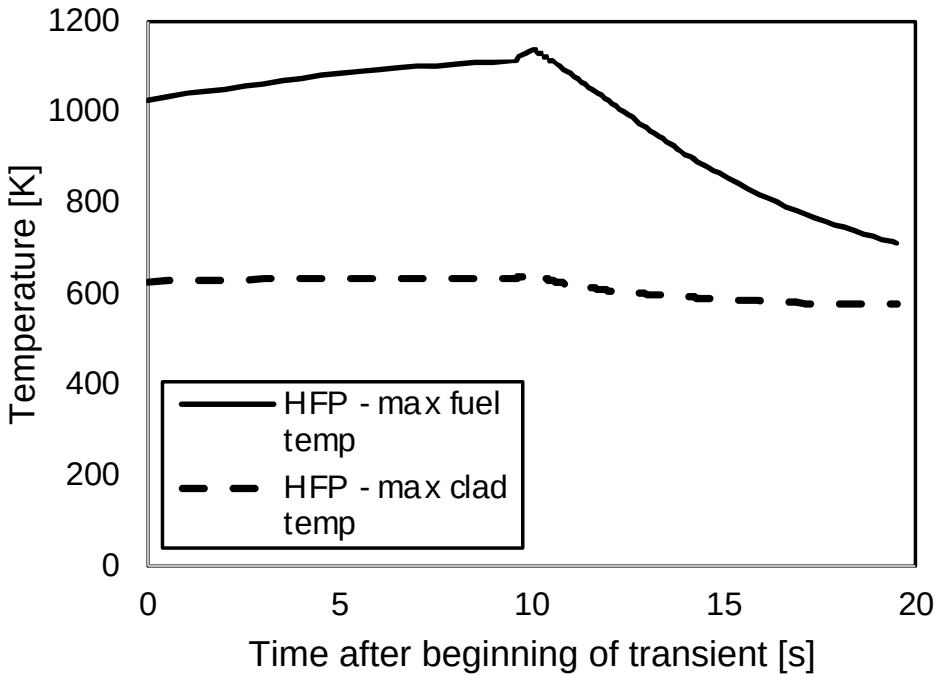


Figure 13. A11-1-1 maximum cladding and fuel temperatures during HFP CRE.

The fuel temperature is below the fuel melting point, 2,700 K, by a significant margin. The maximum cladding temperature is limited to 1,478 K by coolability constraints (as indicated by the SRP), which is not approached in this scenario. There is a small increase in plenum pressure during the transient, shown in figure 14. Because the plenum pressure is higher than the system pressure, 15.5 MPa, the radial average enthalpy is limited to 150 cal/g, and the maximum radial average enthalpy observed was 50.4 cal/g. Cladding deformation can be evaluated using the cladding hoop strain, shown in figure 14, where high cladding hoop strain indicates thermal expansion in the fuel region. There is an increase of .09% hoop strain during the transient, which is less than observed during reactor startup in the steady-state analysis.

When considering the fuel failure criteria outlined in the SRP, the fuel cladding is not expected to fail during this scenario. Cladding failure due to PCMI is dependent on oxide thickness and fuel enthalpy rise. In the case of the high oxide thickness, the fuel can experience a rise in enthalpy of 60 cal/g before failure. The maximum radial average enthalpy was 50.4 cal/g, during which a rise of only 6.2 cal/g was experienced. The 50.4 cal/g maximum radial average enthalpy is also below the 230 cal/g coolability limit. Fuel melt is not experienced, and low hoop strains indicate there was not ballooning that would limit coolability.

IFBA HZP CRE

The power conditions for the most limiting pins in the HZP CRE scenario are shown in figure 15, and each will be analyzed in the future. For now, three pins of interest will be discussed, which are the pins from the highest burnup assembly on the edge of the core, the highest burnup assembly from the center region of the core, the peak power assembly, the maximum fuel temperature assembly, and the maximum fuel temperature rise assembly.

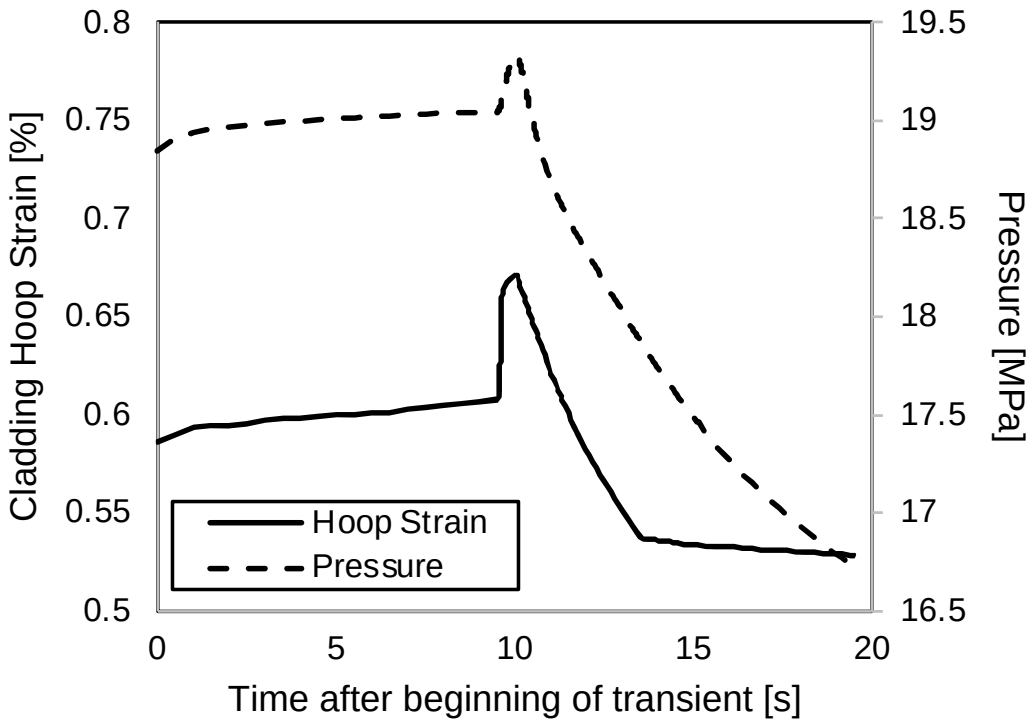


Figure 14. A11-1-1 plenum pressure and cladding hoop strain during HFP CRE.

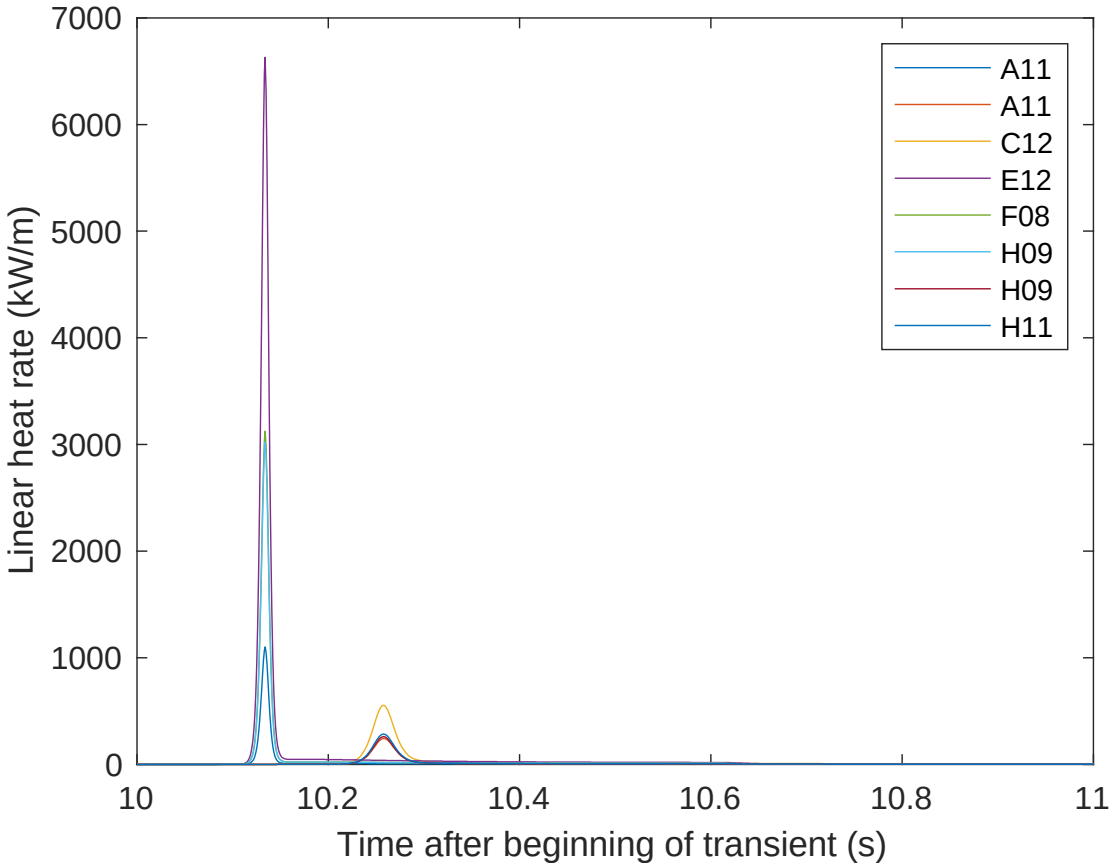


Figure 15. LHR for pins of interest during HZP CRE.

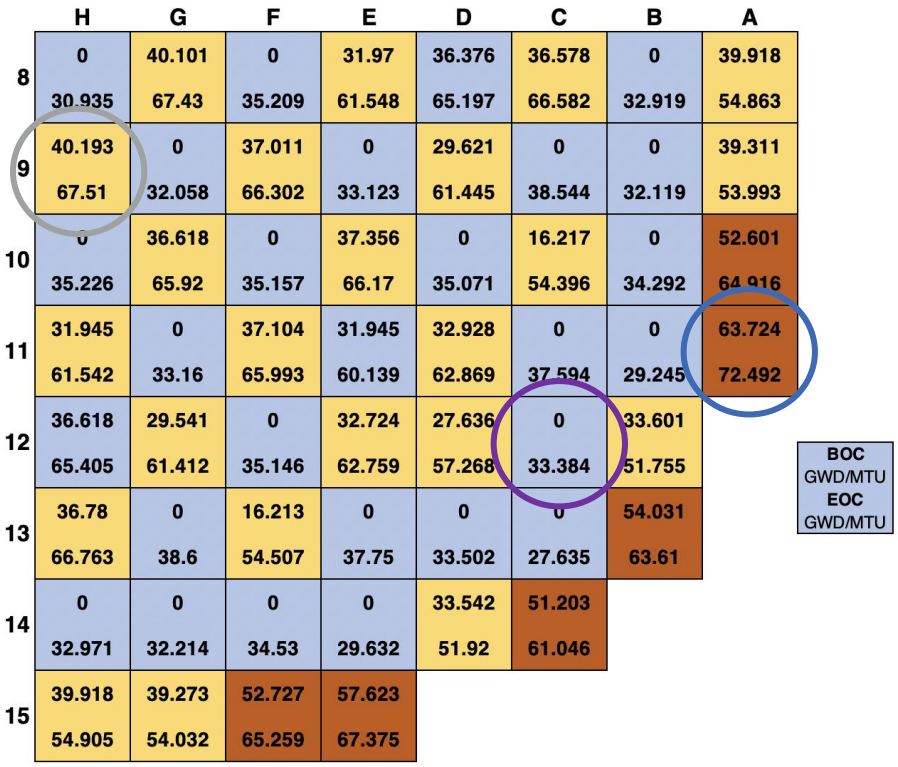


Figure 16. Selected assemblies of interest for HZP CRE analysis.

Those assemblies are H09 for the highest burnup from the center region, A11 for the highest burnup in the periphery region, and C12 for the remaining pins of interest. These assemblies are highlighted in figure 16 and the power pulse experienced by each of the selected pins is shown in figure 17.

Figure 18 shows the maximum fuel temperature during the transient experienced by each pin. The temperature rise directly correlates to the power level during the transient, as expected. The maximum temperature reached overall was in pin C12 and it reached ~2500K. A safety limit outlined in the FSAR is that the fuel can experience <10% fuel melting, with fuel melting occurring at 2700-2800 K. The maximum fuel temperature observed is comfortably below the melting point, so this safety limit is not a concern as of right now.

Figure 19 shows the cladding hoop strain of each pin during the transient. A hoop strain result that is interesting is the C12 result, which is the highest energy deposition case. Instead of decreasing after the power pulse concludes like the other pins, C12 continues to increase for a few seconds before decreasing as expected. This is due to the high temperatures reached in the cladding, which is a result of heat transfer from the fuel. In this simulation, the fuel produced enough heat for the cladding to heat significantly, shown in figure 20, causing thermal expansion. This also pushes the cladding hoop strain over 1%, which is the range where cladding failure is more likely. While the SRP limits the cladding hoop strain to 1% during steady state operation and AOOs, this scenario is a DBA and thus failure is admissible and needs to be considered in the radiological release portion of the safety analysis.

Table 2 summarizes the maximum radial average enthalpy and maximum radial average enthalpy rise in each of the pins. The maximum was found by having BISON output the radial average enthalpy at the height of the largest peaking factor at each timestep.

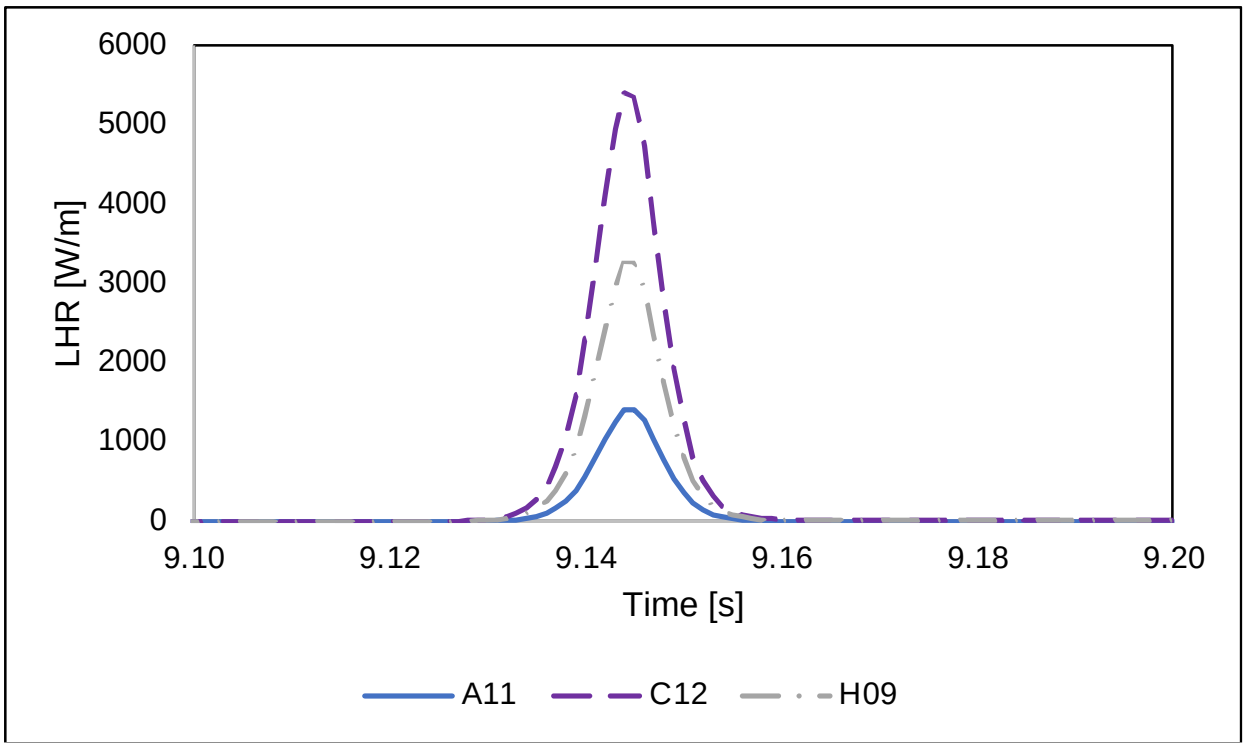


Figure 17. LHR experienced for each pin of interest in HZP CRE.

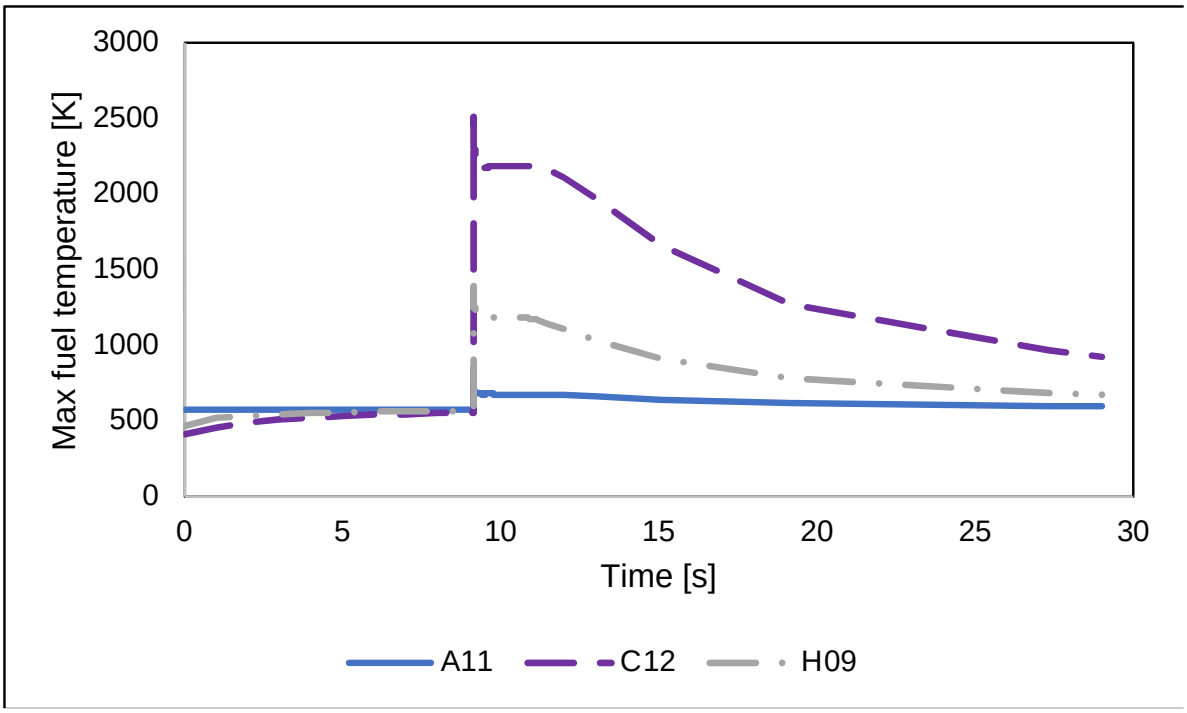


Figure 18. Maximum fuel temperature of each pin of interest during HZP CRE.

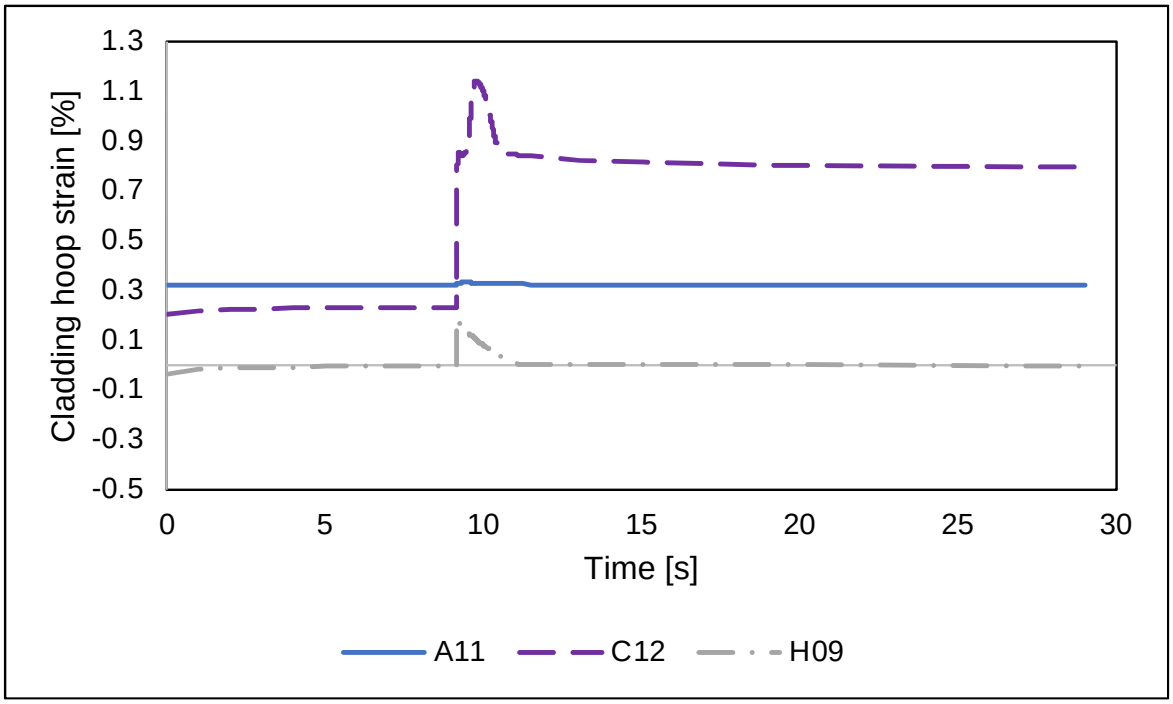


Figure 19. Cladding hoop strain of each pin of interest during HZP CRE.

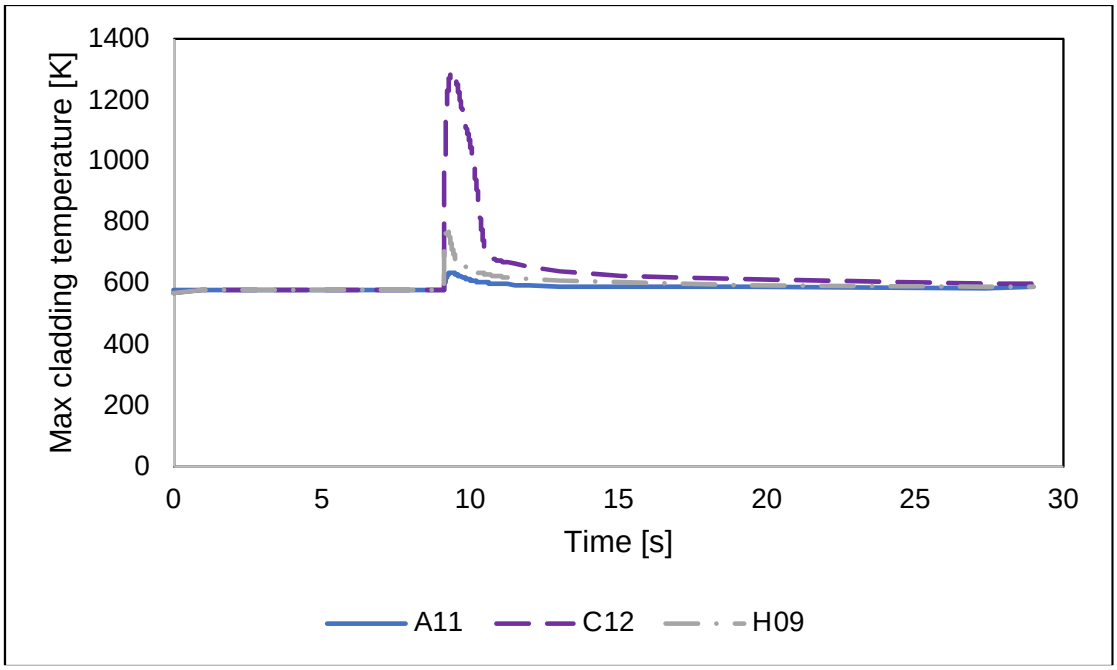


Figure 20. Maximum cladding temperature for each pin of interest during HZP CRE.

Table 2. Enthalpy rises experienced for each pin of interest during HZP CRE

	Number of Cycles	Max radial average enthalpy [cal/g]	Max radial average enthalpy rise [cal/g]
A11	3	32.21	7.02
H09	2	63.80	52.03
C12	1	136.91	126.21

At this power peak, the maximum value throughout the transient was found. The maximum rise was found by subtracting the radial average enthalpy at the same height at the beginning of the transient from the maximum value.

When considering safety limits outlined in NUREG-800, the maximum radial average enthalpy rise is what is considered. The maximum value from all four simulations was from pin C12, with a value of 126.21 cal/g. It is expected that cladding of 30 GWd/MTU should have a hydrogen content of about 200 ppm. Proposed regulatory guides use a relationship between enthalpy rise and hydrogen content to determine cladding failure, as shown in figure 21, which has been reproduced from Regulatory Guide 1.236 [51]. Using this relationship, it can be assumed C12 is likely to fail. As mentioned earlier, this scenario is a DBA and thus failure is admissible and needs to be considered in the radiological release portion of the safety analysis. However, cladding failure is not favorable as the cladding is first defense against fission product release.

MIT proposed annular, blended gadolinium fuel design

To perform a complete analysis that compares fuel designs, the same analysis described in the IFBA section was performed with the annular, gadolinium doped fuel design. For each scenario, the pins that experience the highest burnup in the periphery, the highest burnup in the center of the core, the highest power, the highest fuel temperature, and the highest fuel temperature rise was selected as pins of interest, shown in table 3.

MIT Steady state

Figure 22 shows the steady state LHR history for each of the pins of interest. In total, there are 33 pins of interest. The necessary parameters to consider when considering licensing limitations during steady state operation are fuel temperature, cladding temperature, rod internal pressure, and hoop strain.

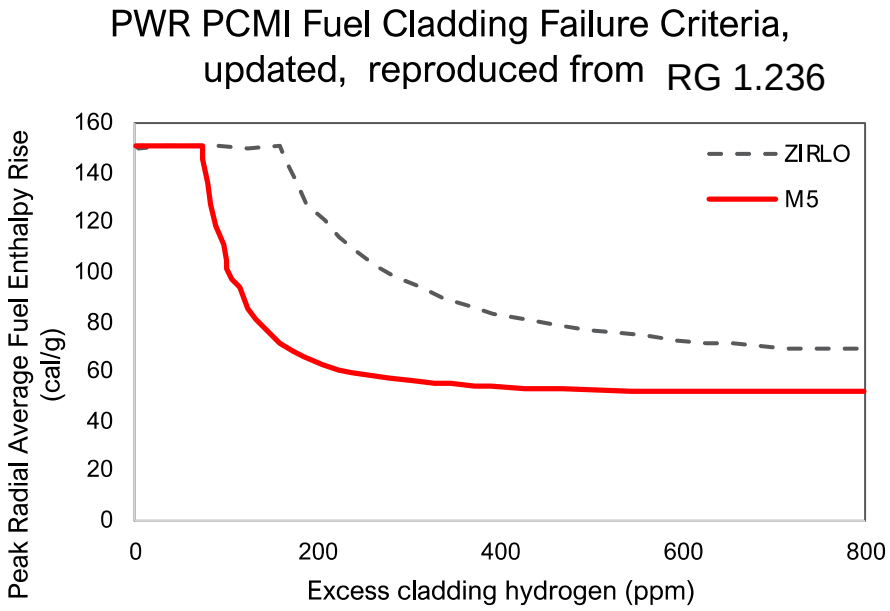


Figure 21. Cladding failure as a function of peak radial average fuel enthalpy rise and excess cladding hydrogen [51].

Table 3. Pins of interest for gadolinium analysis.

Pins of Interest				
Case	HFP CRE	HFP CRW	HZP CRE	HZP CRW
Peak burnup (periphery)	E15	E15	E15	E15
Peak burnup (center)	H13	H13	H13	H13
Peak Power	C09	C12	D08	C09
Avg Power	C13	D10	D12	C13
Peak Temp	C09	C09	D08	C09
Peak Temp Rise	H08	G09	D08	C09

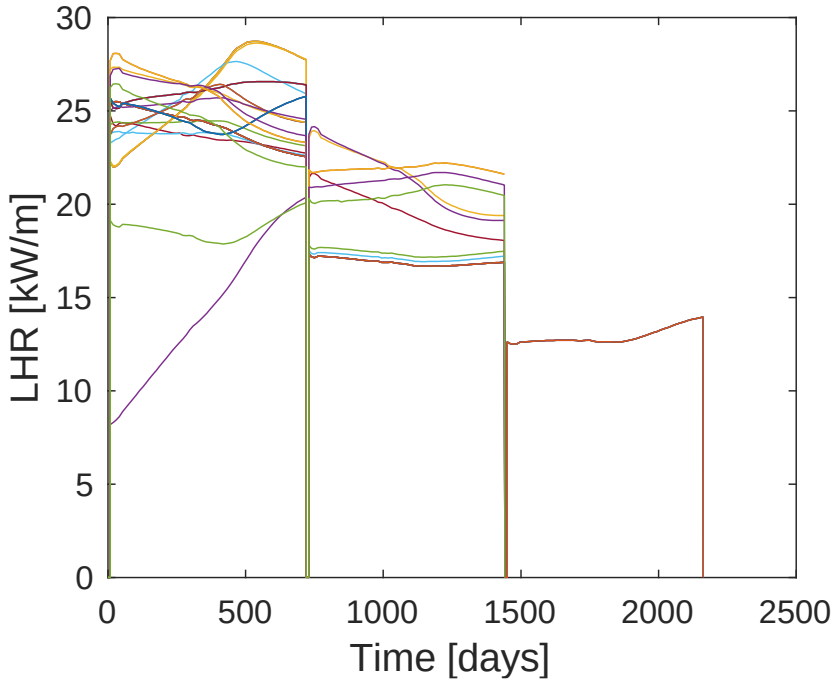


Figure 22. LHR history for each pin of interest for gadolinium steady state analysis

Figure 23 shows the maximum fuel temperature for all pins throughout steady state and figure 24 shows the maximum cladding temperature for all pins throughout steady state. The highest temperature observed across all fuel pins was 1922 K in C09. Heat transfer properties through the gap region and the outer region of the fuel degrade over the life of the fuel due to build up of fission products and morphological changes to the fuel as burnup increases. This degradation causes the fuel centerline temperature to increase throughout each cycle, even though the LHR generally remains the same or decreases. The observed temperature is notably higher than the temperatures observed in the IFBA portion of this work, however this is to be expected due to the lower conductivity of gadolinium doped fuel, even though the maximum power observed in this design is similar to the maximum power observed in the IFBA core. All cladding temperatures are similar to one another, with a maximum of 658 K observed. Both of these values are well within limitations set by regulatory guidance.

Figure 25 shows the rod internal pressure of each pin throughout steady state operation. Rod internal pressure increases throughout each fuel cycle due to the release of fission gas and thermal expansion of the fuel. All but two pins maintained rod internal pressures that were below system pressures, with the maximum observed being 17.98 MPa. Because these two pins are above system pressure, further analysis is necessary to ensure cladding liftoff does not occur, reorientation of hydrides in the radial direction does not occur, and DNB does not occur.

Figure 26 shows the evolution of hoop strain throughout steady state operation. The cladding hoop strain initially decreases due to cladding creepdown under the coolant system pressure. Compressive hoop strain is observed in the first fuel shuffle sequence as a result of the decrease in temperature. During the second and third fuel cycles, the gap region is closed, and an expanding hoop strain is observed. As the fuel thermally expands in the radial direction, strain

increases. Similar to the first fuel shuffle sequence, a decrease in cladding hoop strain is observed during the second fuel shuffle sequence due to the decrease in fuel temperature. All hoop strains are below 1%, satisfying the regulatory requirements.

MIT Fuel Design Transient Results

This section discusses the results of the selected transients for the annular, gadolinium fuel design. It has been established that hot zero power conditions are more severe than hot full power conditions. For this reason, only hot zero power conditions were analyzed. To understand how the fuel will respond in varying levels of severity, an analysis of a HZP CRW and HZP CRE was performed. The CRW is considered an AOO, while the CRE is considered a DBA.

MIT HZP CRW

As discussed earlier, during an AOO, fuel is expected to return to service. This means that all normal operation safety requirements must be met. When considering the requirements relevant to fuel performance, the simple requirements that should be met are that the fuel should not melt, the cladding should not fail, cladding strain should not exceed 1%, the rod internal pressure should not exceed the system pressure [3].

For the analysis of this transient, PARCS provided the transient fuel LHR behavior, shown in figure 27, and fuel axial peaking factors for each pin of interest to RELAP5-3D. RELAP5-3D provided the coolant boundary conditions, temperature, and pressure to BISON, along with the power profile from PARCS. To capture a range of behaviors, five pins of interest were selected by significant results from the PARCS simulation from the following assemblies:

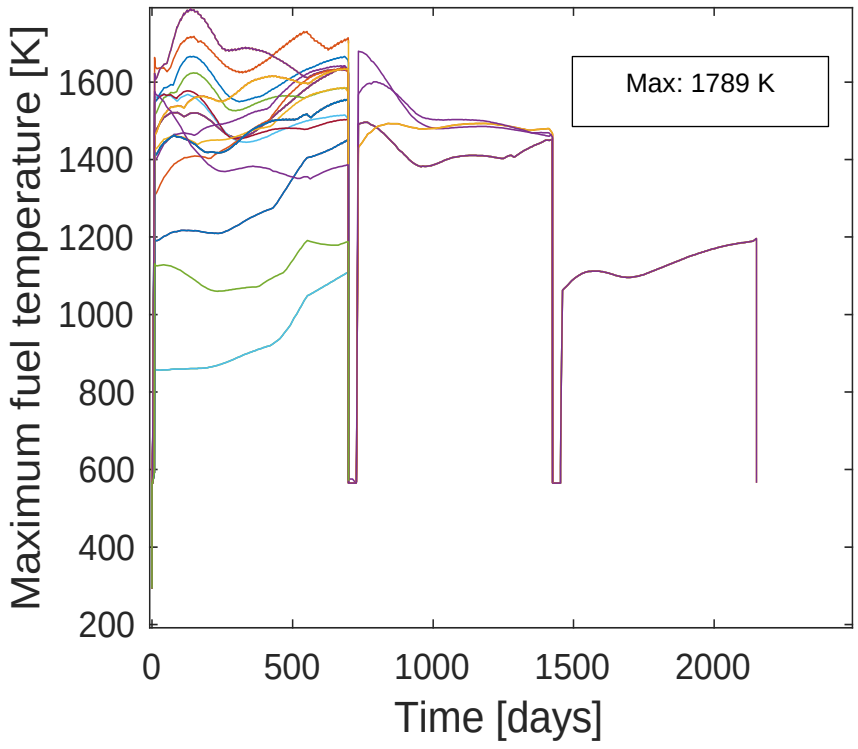


Figure 23. Maximum fuel temperature for all pins throughout steady state

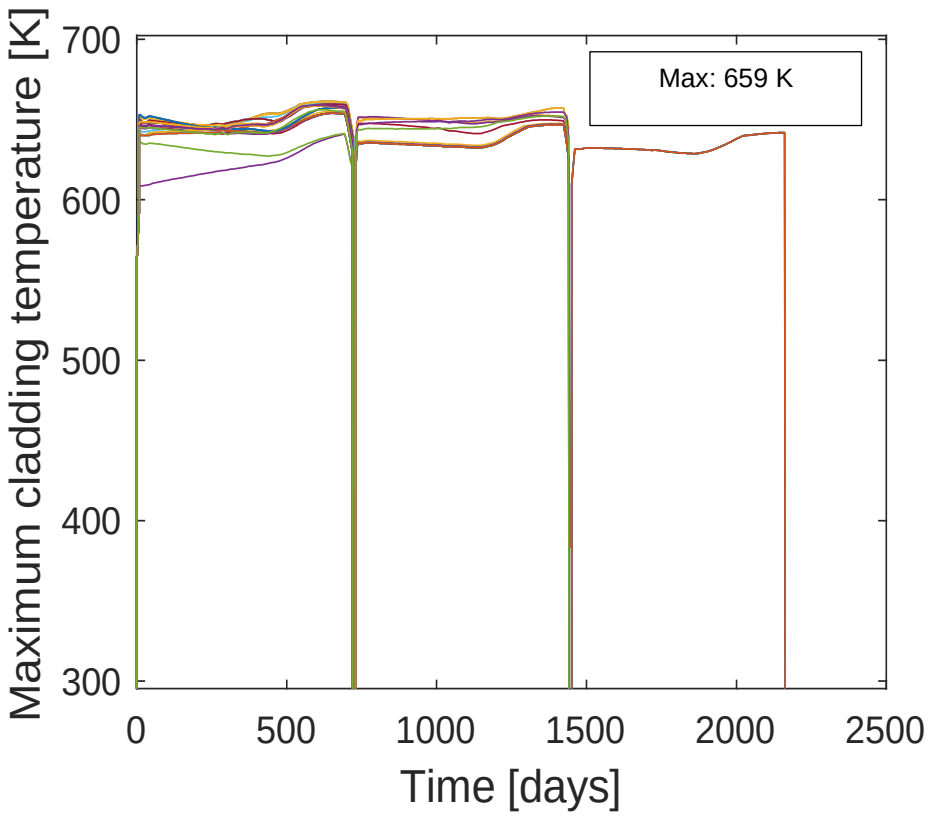


Figure 24. Maximum cladding temperature for all pins of interest throughout steady state

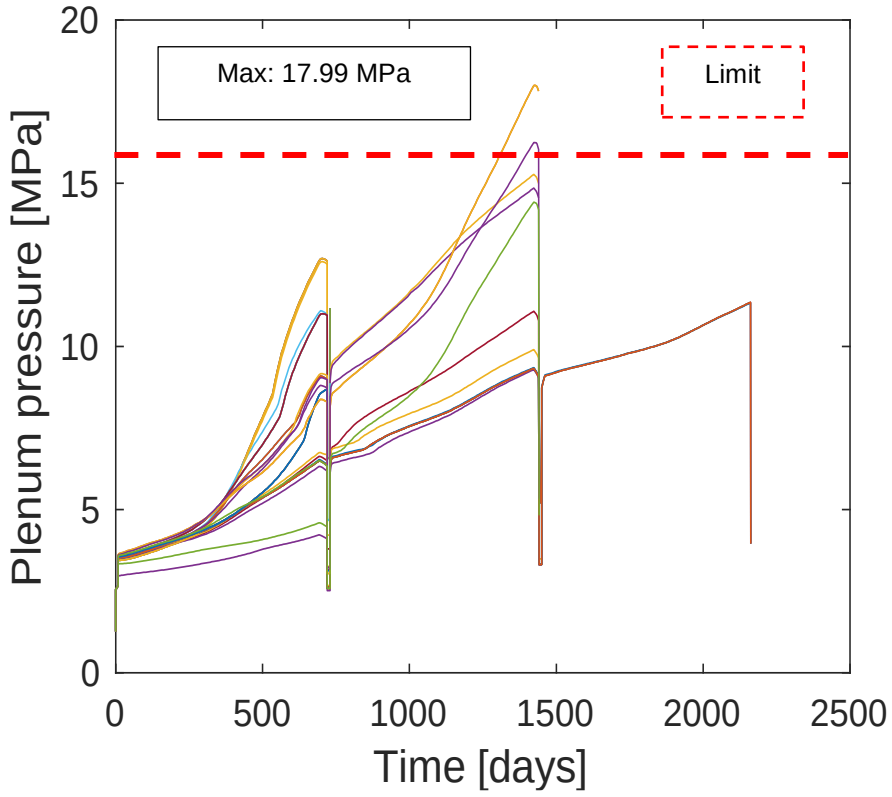


Figure 25. Rod internal pressure for each pin of interest during steady state operation.

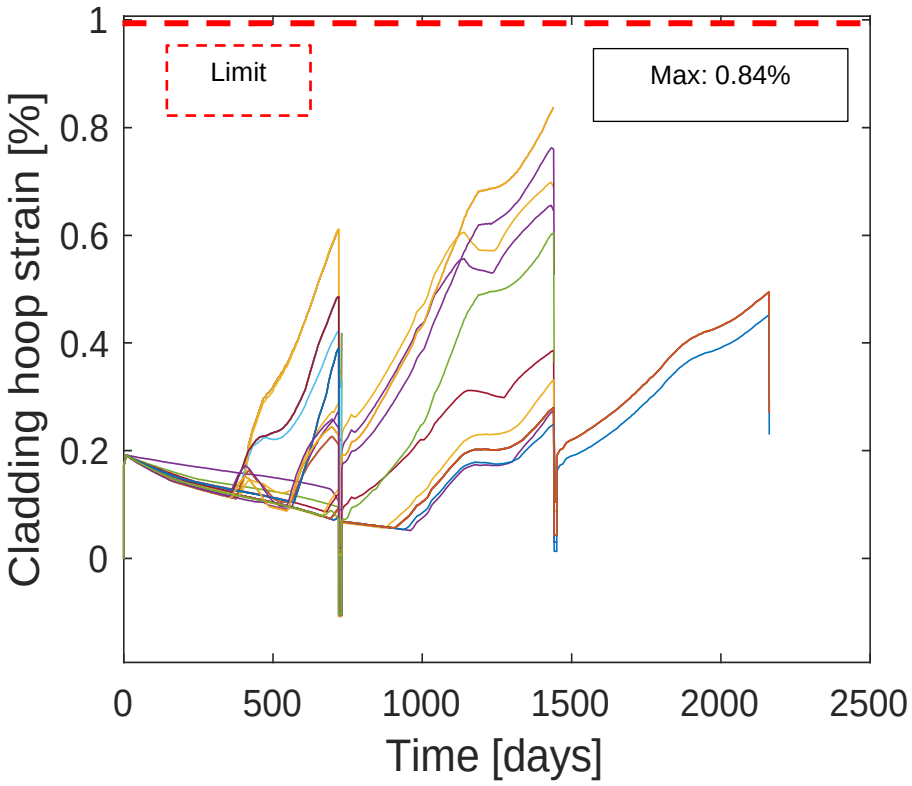


Figure 26. Cladding hoop strain for each pin of interest during steady state.

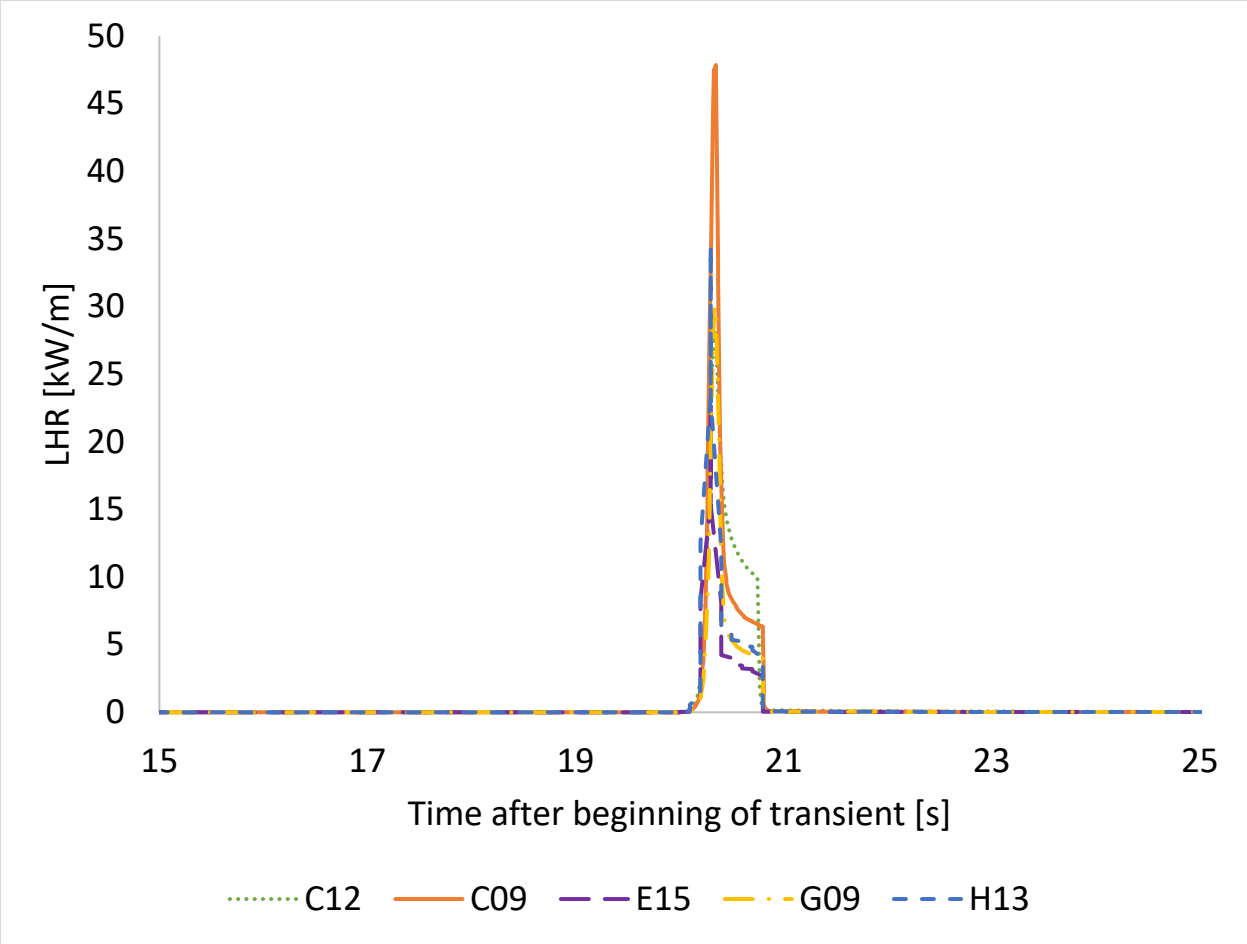


Figure 27. Linear heat rate for HZP CRW for pins of interest.

- E15 – representing highest burnup in the periphery region of the core
- H13 – representing highest burnup in the center region of the core
- G09 – representing peak temperature rise in the fuel
- C09 – representing peak temperature and peak power in the fuel
- C12 – representing peak power of a fresh fuel assembly

Figure 28 shows the maximum temperature of the fuel and figure 29 shows the maximum temperature of the cladding throughout the transient. As expected, the fuel increases in temperature proportionally to the power increase. Out of all scenarios, the most significant temperature was C12, representing the peak power of a fresh fuel assembly, reaching a maximum temperature of 581 K. Understanding that a conservative estimation of the fuel melting point is 2700K and the melting point of gadolinium is 1585 K, this temperature is not challenging to the fuel integrity. The maximum cladding temperature reached across all simulations was in pin G09, which represents the peak power pin, and was 598 K. Coolability requirements limit cladding temperatures to below 1478 K, therefore this transient is not challenging to the cladding from a temperature standpoint.

Cladding failure can be assessed by the radial average enthalpy rise. Across all simulations, the maximum radial average enthalpy rise was 14.94 cal/g. In the most conservative failure criteria, cladding could fail at 60 cal/g with high hydrogen concentration, therefore it is unexpected the cladding fail in this scenario. Figure 30 shows the hoop strain throughout the transient. The maximum hoop strain experienced during this transient was 0.44%, which is comfortably below the 1% hoop strain limit. Figure 31 shows the plenum pressure throughout the transient. The maximum pressure observed across all pins of interest was 9.56 MPa, which is below the system pressure, 15.5 MPa, by a significant margin.

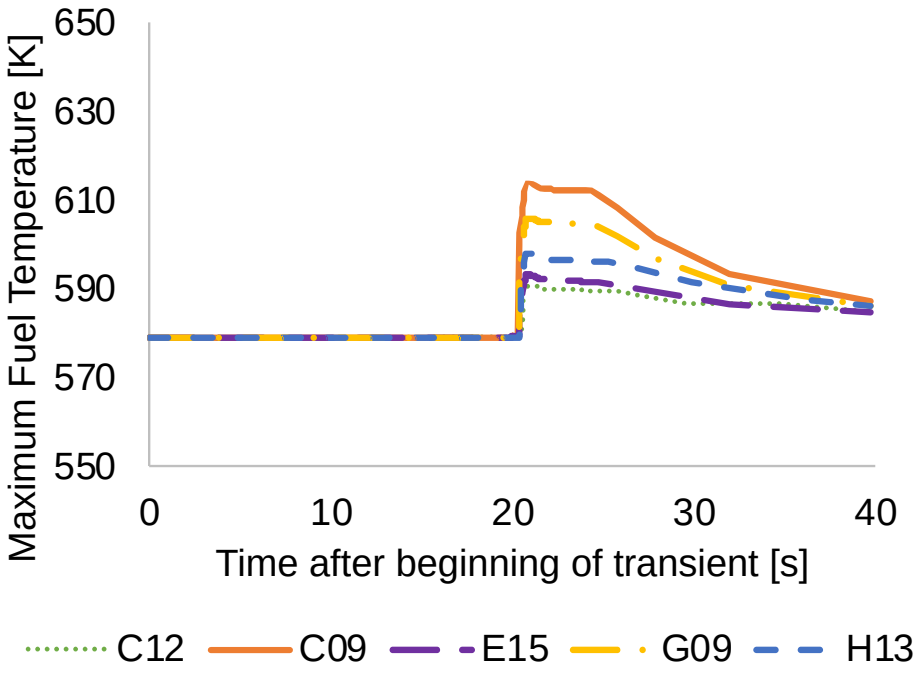


Figure 28. Maximum fuel temperature for pins of interest during HZP CRW.

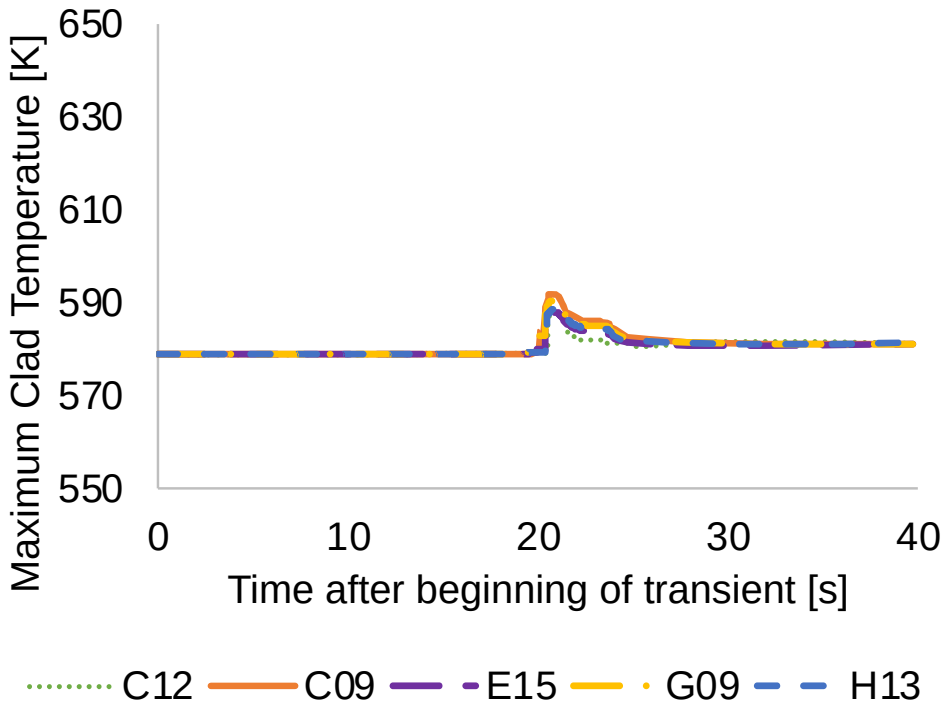


Figure 29. Maximum cladding temperature during HZP CRW for pins of interest.

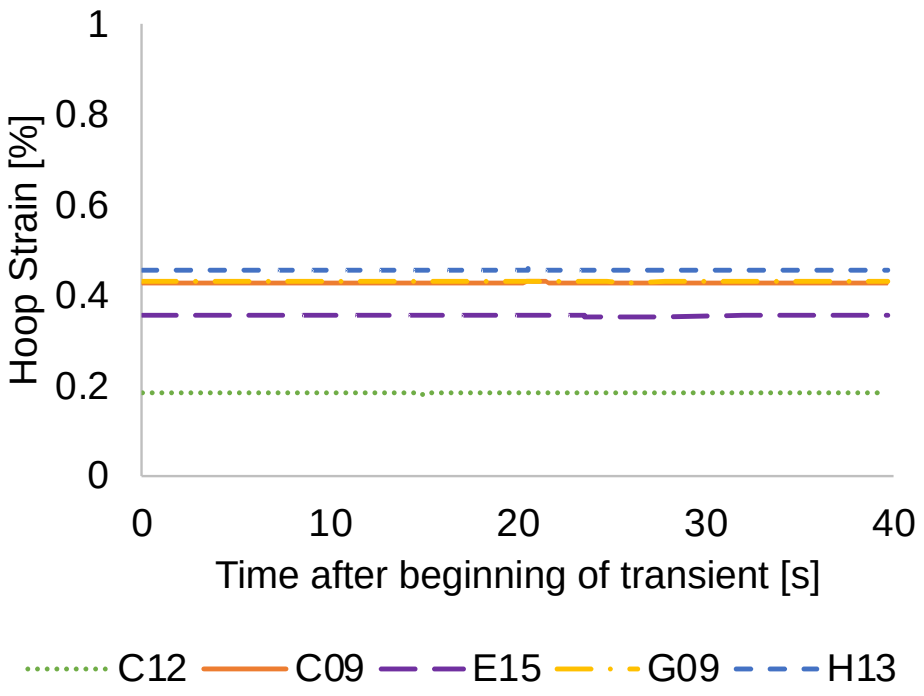


Figure 30. Maximum cladding hoop strain during HZP CRW for pins of interest.

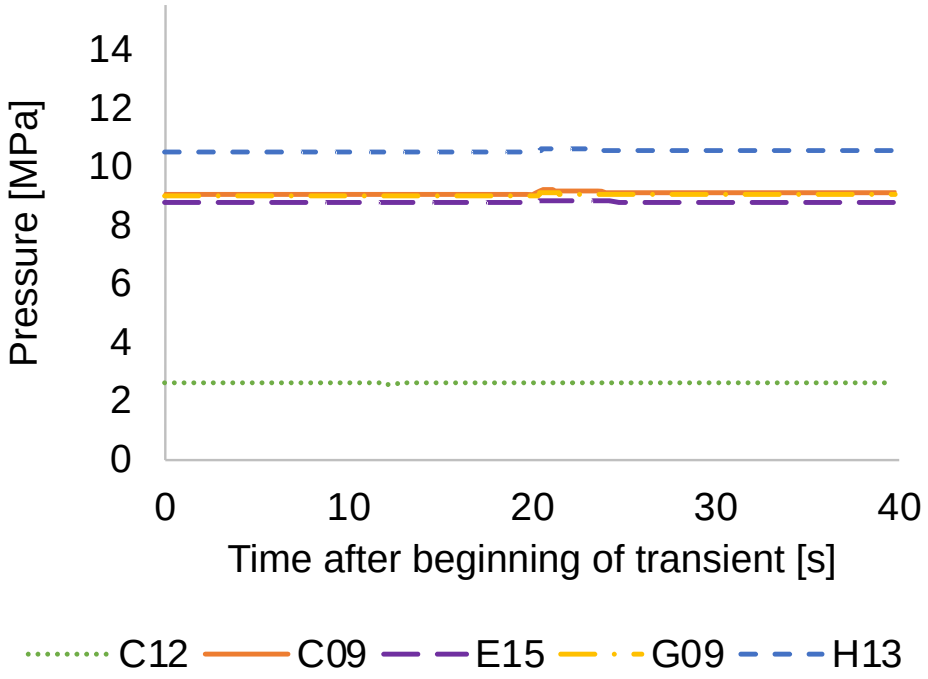


Figure 31. Plenum pressure during HZP CRW for pins of interest.

MIT HZP CRE

As discussed earlier, a CRE is considered a DBA, where different limitations are applicable. Unlike during an AOO, it is permissible that up to 10% of the fuel can melt and the cladding can fail. However, coolability of the fuel should be maintained. Coolability conditions for the fuel can be summarized by a 1478 K limit for the cladding, the general avoidance of cladding failure, and an radial average enthalpy limit of 230 cal/g.

For the analysis of this transient, PARCS provided the transient fuel LHR behavior, shown in figure 32, and fuel axial peaking factors for each pin of interest to RELAP5-3D. RELAP5-3D provided the coolant boundary conditions, temperature, and pressure to BISON, along with the power profile from PARCS. To capture a range of behaviors, five pins of interest were selected by significant results from the PARCS simulation from the following assemblies:

- E15 – representing highest burnup in the periphery region of the core
- H13 – representing highest burnup in the center region of the core
- D08 – representing peak temperature and peak power in the fuel
- E10 – representing average power
- B09 – representing a fresh fuel assembly

Figure 33 shows the maximum temperature of the fuel and figure 34 shows the maximum temperature of the cladding throughout the transient. As expected, the fuel increases in temperature proportionally to the power increase. Out of all scenarios, the most significant temperature was D08, representing the peak power of a fresh fuel assembly, reaching a maximum temperature of 1410 K. Understanding that a conservative estimation of the fuel melting point is 2700K and the melting point of gadolinium is 1585 K, this temperature is not challenging to the fuel integrity.

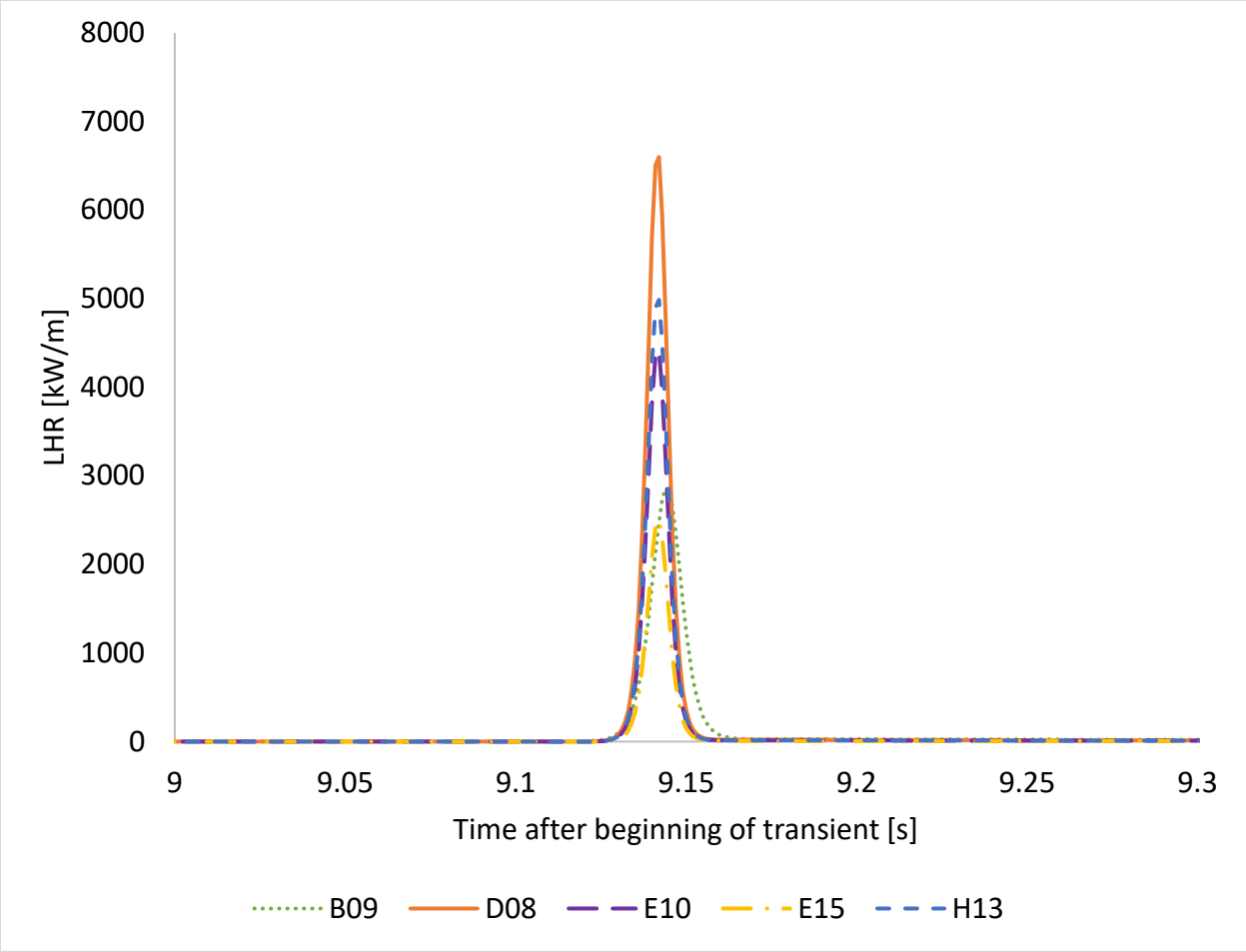


Figure 32. Power history for HZP CRE pins of interest.

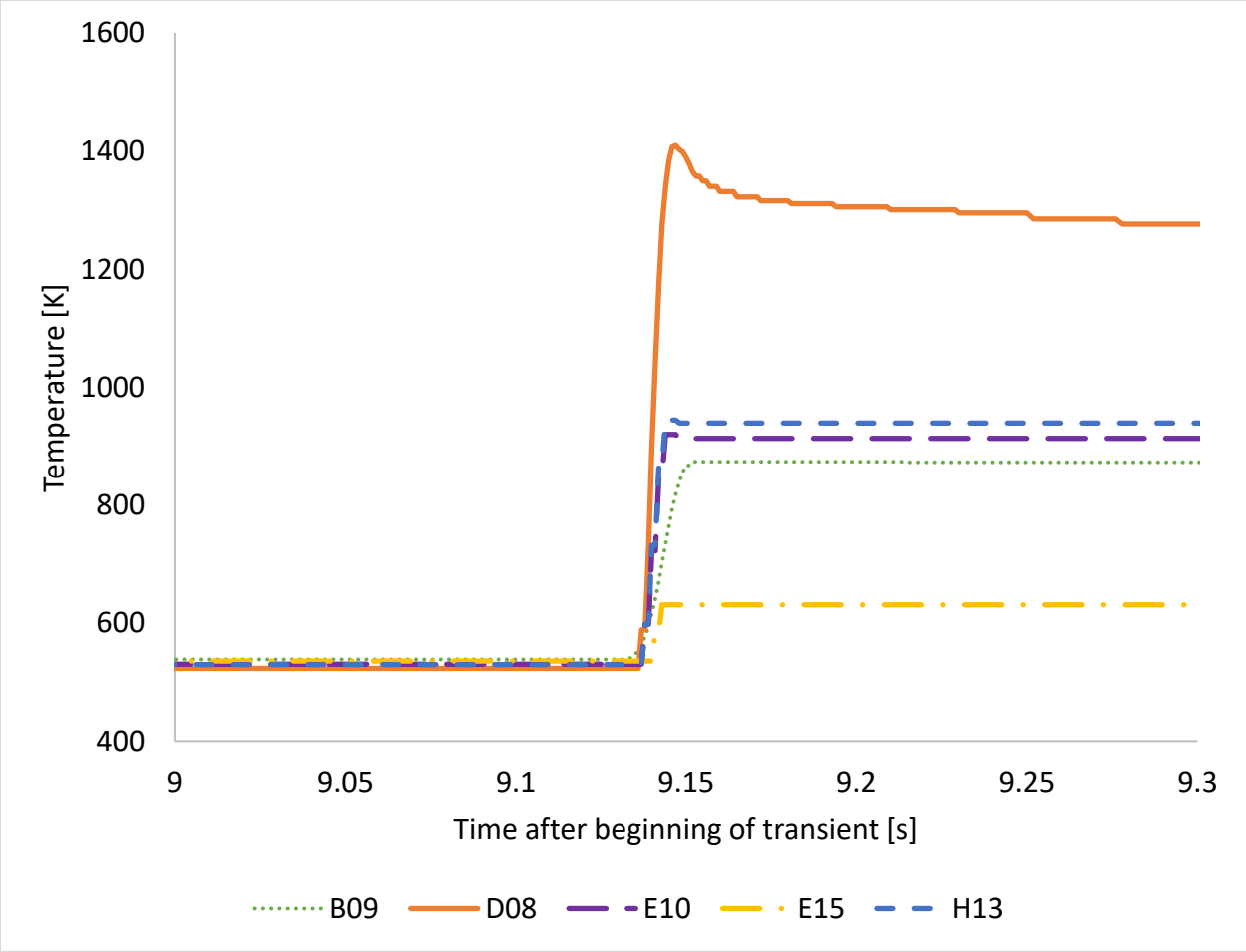


Figure 33. Maximum fuel temperature observed during HZP CRE for pins of interest.

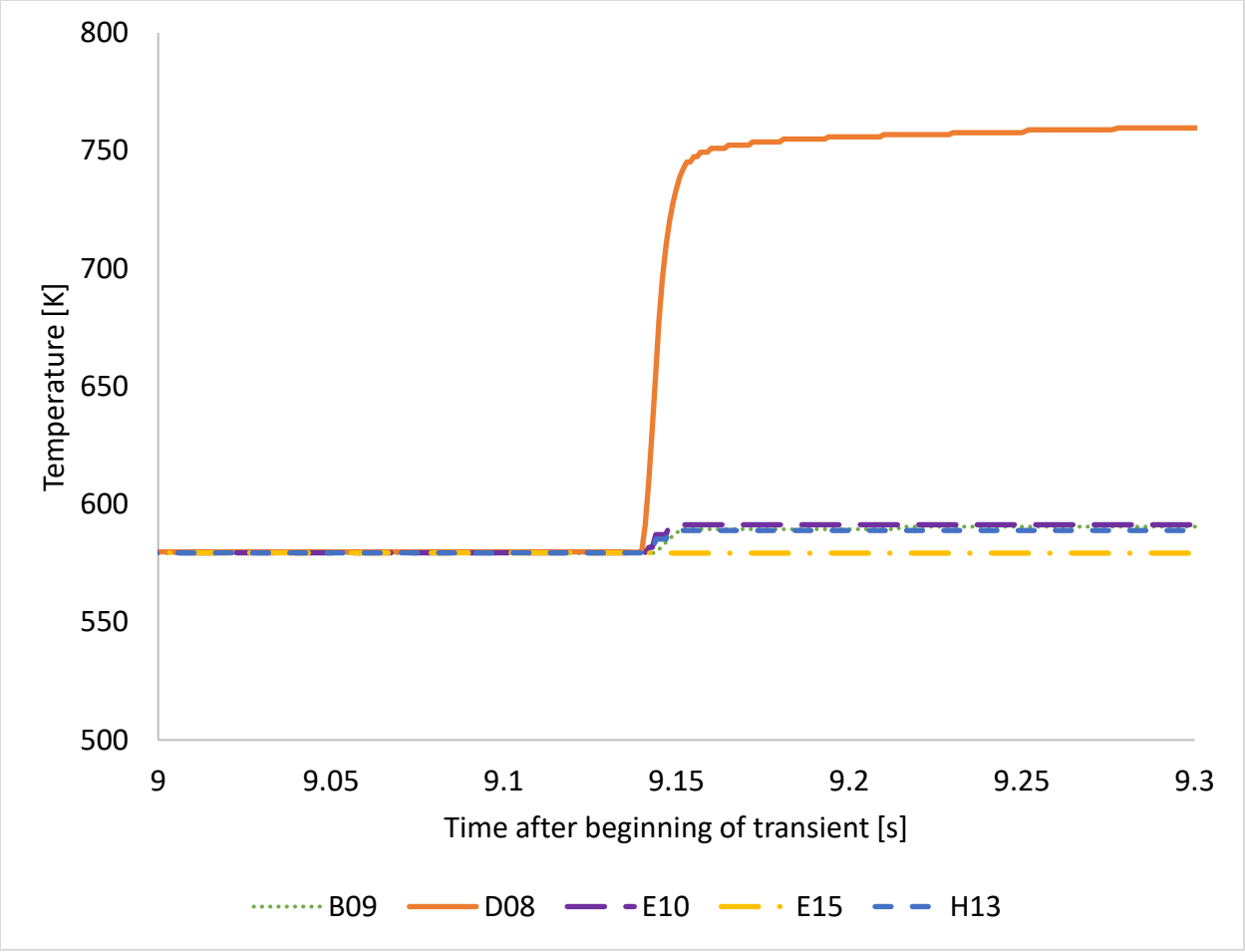


Figure 34. Maximum cladding temperatures observed during HZP CRE for pins of interest.

The maximum cladding temperature reached across all simulations was also in pin D08, which represents the peak power pin, and was 742 K. Coolability requirements limit cladding temperatures to below 1478 K, therefore this transient is not challenging to the cladding from a temperature standpoint.

Cladding failure can be assessed by the radial average enthalpy rise. Across all simulations, the maximum radial average enthalpy rise was 48.27 cal/g. In the most conservative failure criteria, cladding could fail at 60 cal/g with high hydrogen concentration, therefore it is unexpected the cladding fail in this scenario. The overall maximum radial average enthalpy was 60.12 cal/g, which is significantly below the 230 cal/g coolability limit. Figure 35 shows the hoop strain throughout the transient. The maximum hoop strain experienced during this transient was 0.61%, which is comfortably below the 1% hoop strain failure limit that is enforced for normal operation.

Figure 36 shows the plenum pressure throughout the transient. The maximum pressure observed across all pins of interest was 11.26 MPa, which is below the system pressure, 15.5 MPa, by a significant margin.

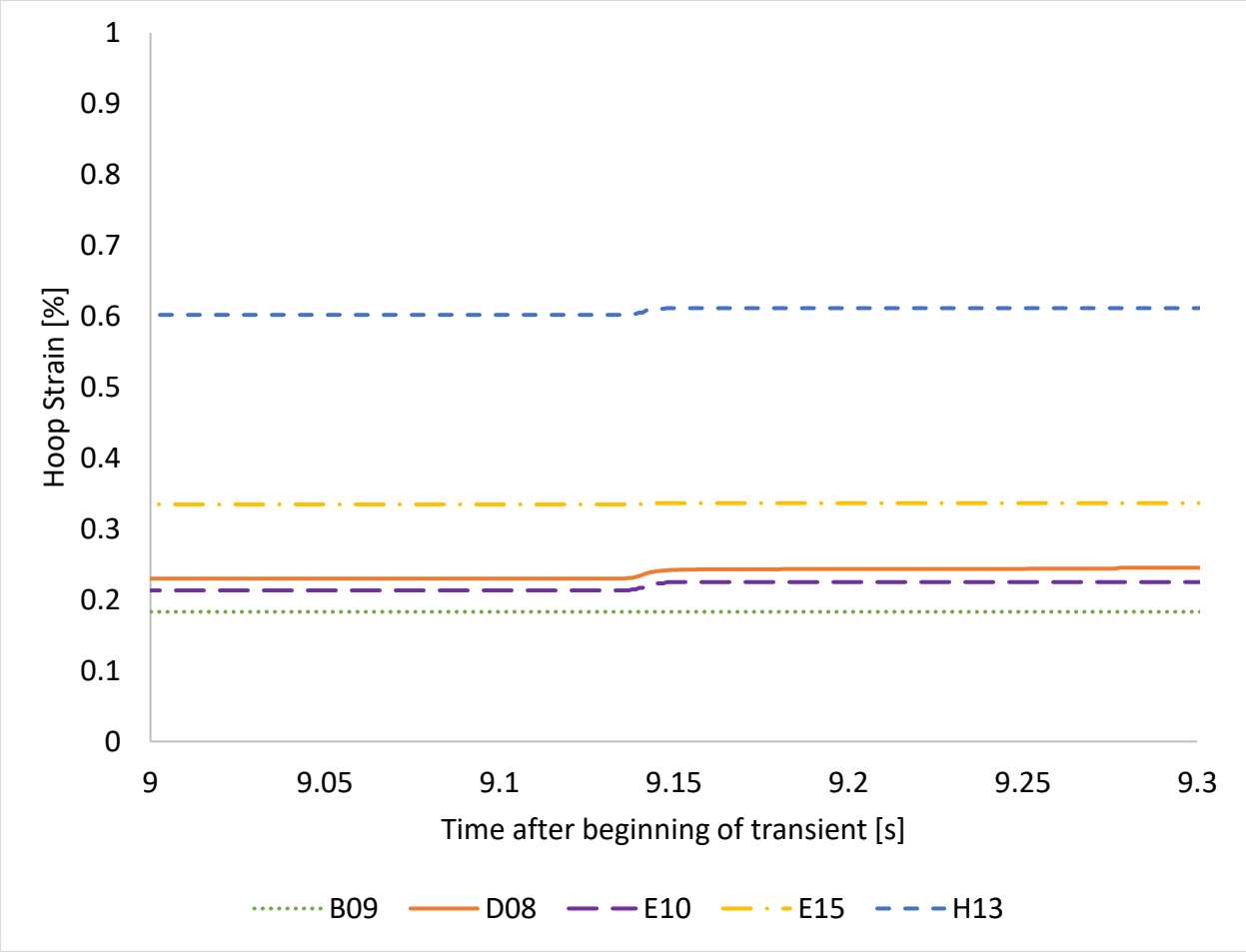


Figure 35. Maximum cladding hoop strains observed for pins of interest during HZP CRE.

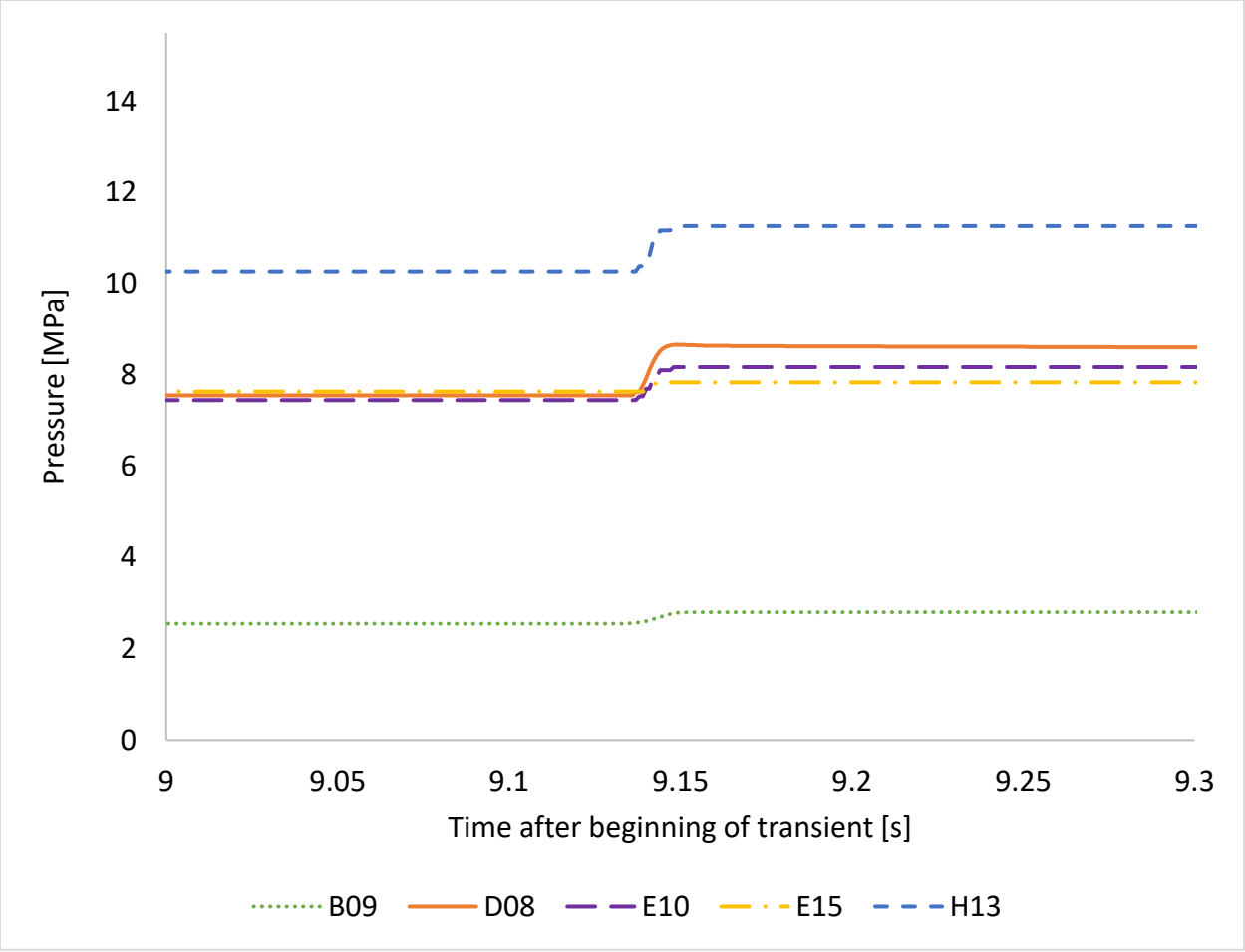


Figure 36. Plenum pressure observed for pins of interest during HZP CRE.

CHAPTER FIVE - CONCLUSIONS AND DISCUSSION

The key questions of this work were

1. Is the current Westinghouse IFBA fuel design with increased enrichment up to 6.6 wt% and burnup up to 73 GWd/MTU sufficient to meet design requirements?
2. Is the MIT annular, gadolinium doped fuel design acceptable in a 24-month cycle?
3. What are the significant lessons learned from the two fuel designs?

To address these questions, analyses were performed on steady state operation, selected AOOs, and selected DBAs. This work employed a loose coupling of PARCS, RELAP5-3D, and BISON to obtain a core-wide understanding of fuel behavior during these scenarios.

From the results shown in this work, summarized in table 4, a conservative conclusion to question 1 is no, the current Westinghouse IFBA fuel design with increased enrichment is insufficient to meet design requirements. During steady state operation, both CRW scenarios, and HFP CRE, the fuel performs adequately, satisfying design criteria described in the SRP. However, during HZP CRE conditions, a pin from assembly C12 demonstrated a possibility of failure due to the average radial enthalpy rise. Although during a DBA cladding failure is permissible, it is nonetheless undesirable and requires continued radiological release analyses in order to be permittable.

However, addressing question 2, the MIT annular fuel design satisfies all requirements comfortably. During steady state operation, all temperature, pressure, and hoop strain requirements are satisfied. Among all transient scenarios, the maximum fuel temperature observed was 1410 K, which is under the limit of 2700 K by a large margin. The largest cladding temperature observed was 724 K, which is an order of magnitude below the regulatory limit. Additionally, the largest enthalpy rise was only 48.27 cal/g and the largest enthalpy insertion was

60.12 cal/g. Lastly the greatest plenum pressure observed was 11.26 MPa, which is significantly below the operational system pressure. Using these results, it can be concluded that this fuel type is acceptable for the proposed core design.

There are a few lessons learned from this work. The first is that the high burnup structure may not be the most impactful factor when considering a full core design. Because it takes several fuel cycles to reach burnup levels greater than 40 GWd/MTU, the level at which high burnup structure begins to develop in the fuel, the fuel with the highest burnups have been sufficiently depleted and have likely been shuffled to the outer periphery region of the core. The fuel at the edge of the core is less sensitive to RIA type transients due to their distance from the removed control rod, whether withdrawn or ejected, and due to their levels of depletion. Instead, pins that had 1-2 cycles worth of depletion that were still near the center region of the core exhibited more significant behavior. This is due to their relatively close proximity to the removed control rod and a higher fissile material content.

The next learned lesson is that the type of burnable absorber implemented plays a significant role on the fuel performance. In the IFBA analyses, there was a large initial increase in plenum pressure due to the release of helium as the boron depleted from the fuel. This initial increase pushed plenum pressures above system operational pressures consistently, which is still licensable, but undesirable. This increased plenum pressure leads to higher cladding stress and strain levels, which are indicators of cladding failure. With the implementation of blended gadolinium, pressures above operational pressures were only observed in two of the selected fuel pins, which is more manageable to address.

Table 4. Summary of the most strenuous fuel performance results compared to NRC guidance.

	Normal operation			CRE		
Core design	IFBA	MIT	Limit	IFBA	MIT	Limit
Fuel temperature	1789 K	1922 K	2700 K	2450 K	1410 K	2700 K
Cladding temperature	665 K	659 K	1478 K	1268 K	760 K	1478 K
Plenum pressure	23.09 Mpa	17.99 Mpa	15.5 Mpa	--	--	--
Cladding hoop strain	1.10%	0.084%	1%	--	--	--
Enthalpy	--	--	--	136.91 cal/g	60.12 cal/g	230 cal/g
Enthalpy rise	--	--	--	126.21 cal/g	48.27 cal/g	RG 1.236 dependent

LIST OF REFERENCES

[1] J. R. Burns, R. Hernandez, K. A. Terrani, A. T. Nelson and N. R. Brown, "Reactor and fuel cycle performance of light water reactor fuel with 235U enrichments above 5%," Annals of Nuclear Energy, vol. 142, p. 107423, 2020.

[2] K. J. Geelhood, "Fuel Performance Considerations and Data Needs for Burnup above 62 GWd/MTU," Pacific Northwest National Laboratory., 2019.

[3] U.S. Nuclear Regulatory Commission, "Standard review plan for the review of safety analysis reports for nuclear power plants. In: LWR Edition," U.S. Nuclear Regulatory Commission, Office of Nuclear Reactor Regulation, 2007.

[4] IAEA, "CORROSION OF ZIRCONIUM ALLOYS IN NUCLEAR POWER PLANTS," IAEA, Vienna, 1993.

[5] A. T. Motta, A. Couet and R. J. Comstock, "Corrosion of zirconium alloys used for nuclear fuel cladding," Annu. Rev. Mater. Res , vol. 45, no. 1, pp. 311-343, 2015.

[6] P. A. C. Raynaud, "Fuel fragmentation, Relocation, and Dispersal during the Loss-of-Coolant Accident," US NRC, 2012.

[7] M. Flanagan, B. C. Oberländer and A. Puranen, "Fuel fragmentation, relocation and dispersal under LOCA conditions: experimental observations.," in In 2013 LWR Fuel Performance Meeting (TopFuel 2013), September 2013.

[8] J. Desquines, D. A. Koss, A. T. Motta, B. Cazalis and M. Petit, "The issue of stress state during mechanical tests to assess cladding performance during a reactivity-initiated accident (RIA)," Journal of Nuclear Materials, vol. 412, no. 2, pp. 250-267, 2011.

[9] A. Bianco, C. Vitanza, M. Seidl, A. Wensauer, W. Faber and R. Macián-Juan, "Experimental investigation on the causes for pellet fragmentation under LOCA conditions," Journal of Nuclear Materials, vol. 465, pp. 260-267, 2015.

[10] K. A. Terrani, "Accident tolerant fuel cladding development: Promise, status, and challenges," Journal of Nuclear Materials, vol. 501, pp. 13-30, 2018.

[11] B. Cox, "Pellet-clad interaction (PCI) failures of zirconium alloy fuel cladding—a review," Journal of nuclear materials, vol. 172, no. 3, pp. 249-292, 1990.

[12] K. Videm, L. Lunde, T. Hollowell, K. Vilpponen and C. Vitanza, "Cracking of cladding tubes caused by power ramping and by laboratory stress corrosion experiments," Journal of Nuclear Materials, vol. 87, no. 2-3, pp. 259-267, 1979.

[13] N. R. Brown, A. J. Wysocki, K. A. Terrani, K. G. Xu and D. M. Wachs, "The potential impact of enhanced accident tolerant cladding materials on reactivity initiated accidents in light water reactors," Annals of Nuclear Energy, vol. 99, pp. 353-365, 2017.

[14] T. Fuketa, H. Sasajima, Y. Mori and K. Ishijima, "Fuel failure and fission gas release in high burnup PWR fuels under RIA conditions," Journal of Nuclear Materials, vol. 248, pp. 249-256, 1997.

[15] T. Nakamura, M. Yoshinaga, M. Takahashi, K. Okonogi and K. Ishijima, "Boiling water reactor fuel behavior under reactivity-initiated-accident conditions at burnup of 41 to 45 GWd/tonne U," Nuclear Technology, vol. 129, no. 2, pp. 141-151, 2000.

[16] T. Nakamura, K. Kusagaya, T. Fuketa and H. Uetsuka, "High-burnup BWR fuel behavior under simulated reactivity-initiated accident conditions," Nuclear technology, vol. 138, no. 3, pp. 246-259, 2002.

[17] F. Schmitz and J. Papin, "High burnup effects on fuel behaviour under accident conditions: the tests CABRI REP-Na," Journal of Nuclear Materials, vol. 270, no. 1-2, pp. 55-64, 1999.

[18] Y. Bibilashvili, N. Sokolov, O. Nechaeva, A. Salatov, F. Sokolov, V. Asmolov, L. Yegorova, E. Kaplar, Y. Trutnev, I. Smirnov and V. Ustinenko, "Experimental Study of VVER High Burn-up Fuel Rods at the BIGR Reactor Under Narrow Pulse Conditions," in In Proc. Int. Topical Meeting on LWR Fuel Performance (CD-ROM), 2000.

[19] A. MacLachlan, "Latest CABRI Test Indicates No Fuel Ejected into Reactor Circuit, Inside N.R.C.," McGraw-Hill Inc., December 18, 2000..

[20] J. Alvis, W. Liu and R. Montgomery, "Fuel Reliability Program: Proposed RIA Acceptance Criteria," Electric Power Research Institute, Palo Alto, CA, 2010.

[21] T. Sugiyama, M. Umeda, T. Fuketa, H. Sasajima, Y. Udagawa and F. Nagase, "Failure of high burnup fuels under reactivity-initiated accident conditions," Annals of Nuclear Energy, vol. 36, no. 3, pp. 380-385, 2009.

[22] Y. Udagawa, M. Suzuki, T. Sugiyama and T. Fuketa, "Stress intensity factor at the tip of cladding incipient crack in RIA-simulating experiments for high-burnup PWR fuels," Journal of nuclear science and technology, vol. 46, no. 10, pp. 1012-1021, 2009.

[23] OECD-NEA, "Nuclear Fuel Behaviour During Reactivity Initiated Accidents, Tech. Rep.," OECD - NEA, 2010.

[24] T. Barani, D. Pizzocri, F. Cappia, L. Luzzi, G. Pastore and P. Van Uffelen, "Modeling high burnup structure in oxide fuels for application to fuel performance codes. part I: High burnup structure formation," Journal of Nuclear Materials, vol. 539, p. 152296, 2020.

[25] OECD-NEA, "RIA Fuel Codes Benchmark - Volume 1," Nuclear Energy Agency of the OECD (NEA), 2013.

[26] OECD-NEA, "Reactivity Initiated Accident (RIA) Fuel Codes Benchmark Phase-II – Volume 1," OECD-NEA, 2016.

[27] O. Marchand, J. Zhang and M. Cherubini, "Uncertainty and sensitivity analysis in reactivity-initiated accident fuel modeling: synthesis of organisation for economic co-operation and development (OECD)/nuclear energy agency (NEA) benchmark on reactivity-initiated accident codes phase-II," Nuclear Engineering and Technology, vol. 50, no. 2, pp. 280-291, 2018.

[28] J. Alvis, W. Liu and K. Yueh, "Fuel Reliability Program: Proposed Reactivity Insertion Accident (RIA) Acceptance Criteria, Revision 1," EPRI, 2015.

[29] G. Khvostov and A. Gorzel, "FALCON code-based analysis of PWR fuel rod behaviour during RIA transients versus new US NRC and current Swiss failure limits," Nuclear Engineering and Technology, vol. 53, no. 11, pp. 3741-3758, 2021.

[30] A. Nawaz, Y. Hidekazu, M. Yang and A. Hussain, "Comparative analysis of RIA and LOCA with and without fuel rod behavior modeling in THEATRe code," Progress in Nuclear Energy, vol. 93, pp. 133-145, 2016.

[31] A. Wysocki, J. Hu, R. Salko and B. Kochunas, "Improvement of CTF for RIA Analysis," in ANS Winter Conference 2020, Oak Ridge, Tennessee, United States of America, Apr 7-9, 2020.

[32] I. Guénot-Delahaie, J. Sercombe, É. Fédérici, C. Bernaudat, R. Largenton and X. Haller, "Investigation of clad ballooning during NSRR RIA tests using ALCYONE fuel performance code," Journal of Nuclear Materials, vol. 562, p. 153584, 2022.

[33] W. Liu, A. Mai, J. Alvis, J. Rashid and C. P. Folsom, "Bison fuel performance modeling on RIA in a PWR," Idaho National Lab.(INL), Idaho Falls, ID, U.S., 2018.

[34] N. Capps, A. Wysocki, A. Godfrey, B. Collins, R. Sweet, N. Brown, S. Lee, N. Szewczyk and S. Hoxie-Key, "Full core loca safety analysis for a PWR containing high burnup fuel," Nuclear Engineering and Design, vol. 379, p. 111194, 2021.

[35] Pavlov, V.I., Sidorenko, V.D., Pozdnyakov, N.E., 1992. Effectiveness of Using Burnable Absorbers in a Vver-1000. Atom Energy+ 73 (6), 977–980.

[36] Evans, J. A., DeHart, M. D., Weaver, K. D., & Keiser, D. D. (2022). Burnable absorbers in nuclear reactors – A Review. Nuclear Engineering and Design, 391, 111726. https://doi.org/10.1016/j.nucengdes.2022.111726

[37] Franceschini, F., Petrovic, B., 2009. Fuel with Advanced Burnable Absorbers Design for the Iris Reactor Core: Combined Erbia and Ifba. Ann Nucl Energy 36 (8), 1201–1207.

[38] Tonks, M., Andersson, D., Devanathan, R., Dubourg, R., El-Azab, A., Freyss, M., Iglesias, F., Kulacsy, K., Pastore, G., Phillpot, S.R., Welland, M., 2018. Unit Mechanisms of Fission Gas Release: Current Understanding and Future Needs. J Nucl Mater 504, 300–317.

[39] IAEA. Characteristics and Use of Urania-gadolinia Fuels. Technical Report IAEA-TECDOC-844, International Atomic Energy Agency, Vienna, Austria, November 1995.

[40] NRC. Nuclear Power Plant Licensing Process, NUREG/BR-0298, Rev 2, Nuclear Regulatory Commission, July 2009

[41] Robertson, J. A. L., “Nuclear Fuel Failures. Their Causes and remedies.” INIS-mf-3193. Vol. 2, 1976, pp. 2-14; Proceedings of CAN/ANS Joing Topical Meeting on Commerical Nuclear Fuel Technology today, Toronto, Canada, April 1975

[42] T. Fuketa, 2.22 e transient response of LWR fuels (RIA), in: Compr. Nucl. Mater, 2012, pp. 579e593, https://doi.org/10.1016/B978-0-08-056033-5.00044-6.

[43] Fuketa, T., Nagase, F., Ishijima, K., Fujishiro, T., “NSRR/RIA Experiments with High-Burnup PWR Fuels”, Nuclear Safety, 37, December 1996.

[44] Idaho National Laboratory, *RELAP5-3D Code Manual Volume I,* Idaho National Laboratory, 2005.

[45] J. Hales, K. Gamble, B. Spencer, S. Novascone, G. Pastore, W. Liu, D. Stafford, R. Williamson, D. Perez, R. Gardner, A. Casagranda, J. Galloway, C. Matthews, C. Unal and N. Carlson, "BISON Users Manual, BISON Release 1.3," Idaho National Laboratory, Idaho Falls, ID, United States, 2016.

[46] Courty, O., Motta, A. T., & Hales, J. D. (2014). Modeling and simulation of hydrogen behavior in zircaloy-4 fuel cladding. Journal of Nuclear Materials, 452(1–3), 311–320. https://doi.org/10.1016/j.jnucmat.2014.05.013

[47] C. Sanders and J. Wagner, Study of the Effect of Integral Burnable Absorbers for PWR Burnup Credit, NUREG/CR-6760, ORNL/TM-2000-321, Oak Ridge National Laboratory, Oak Ridge, Tennessee. 2002.

[48] Nishino Y, Endo M, Ibe E, Yasuda T. Formation and dissolution of oxide film on zirconium alloys in 288 C pure water under g-ray irradiation. J Nucl Mater 1997;248:292e8.

[49] Aly, Z., Casagranda, A., Pastore, G., & Brown, N. R. (2019). Variance-based sensitivity analysis applied to hydrogen migration and redistribution model in Bison. Part I: Simulation of historical experiments. Journal of Nuclear Materials, 524, 90–100. https://doi.org/10.1016/j.jnucmat.2019.06.035

[50] "VEGP-FSAR-15," Nuclear Regulatory Commission, Dec. 2021.

VITA

Isabelle Lindsay graduated from Purdue University with a Bachelor of Science in Nuclear Engineering with a minor in Law and Society in May of 2021. In June of 2021, immediately following graduation, she began graduate research work at the University of Tennessee. Isabelle has presented work at two American Nuclear Society annual meetings in the Nuclear Fuels section and has been accepted to present at the 20th International Topical Meeting on Nuclear Reactor Thermal Hydraulics in August of 2023. Her anticipated graduation date is August of 2023, after which she will begin her pursuit of her Doctor of Philosophy degree in Nuclear Engineering.